International Journal of Hydrogen Energy xxx (xxxx) xxx

Contents lists available at ScienceDirect

International Journal of Hydrogen Energy

journal homepage: www.elsevier.com/locate/he

# Comprehensive evaluation of proton exchange membrane fuel cell-based power system fueled with ammonia decomposed hydrogen

Jiale Yan [a], Jiong Wang [a], Shanshan Cai [a], Chunyan Zang [b,**], Song Li [a,*], Zhengkai Tu [a]

[a] Department of New Energy Science and Engineering, School of Energy and Power Engineering, Huazhong University of Science and Technology, Wuhan, 430074, China
[b] School of Electric and Electronic Engineering, Huazhong University of Science and Technology, Wuhan, 430074, China

ARTICLE INFO

Handling Editor: Prof. A.B. Basile

*Keywords:*
Ammonia decomposition
Fuel cell
Power generation
Energy storage
Hydrogen

ABSTRACT

Proton exchange membrane fuel cell (PEMFC) employing ammonia fuel present a prospective alternative for the operational dynamics of hydrogen fuel cells. Fuel cell systems based on hydrogen production from ammonia decomposition offer several advantages, including low-cost storage and transportation, high safety, high efficiency with low fuel cost, and importantly, are environmentally friendly with no carbon emissions during use. By regulating the hydrogen production from ammonia decomposition and the coordinated control of the PEMFC and energy storage devices, efficient and stable power generation can be achieved. In this study, with the electrical demand of 285 households in a community as the target output, an integrated system comprising an ammonia decomposer, membrane separator and PEMFCs is proposed. The effects of integrating different energy storage devices, including hydrogen tanks and lithium batteries, along with various ammonia decomposition input modes such as hourly, stepped, and constant flow strategies on the system's operation characteristics were systematically analyzed. Furthermore, the overall system performance and economic assessment were conducted, considering the equipment invested and the revenue generated for each strategic approach. It is demonstrated that the regulation strategy with constant flow input exhibited an average system efficiency of 52.49%, outperforming the stepped flow mode-based strategy, and the strategies based on the energy storage of lithium battery operate more stable than the ones based on hydrogen storage tanks. Overall, the strategy with constant flow, lithium battery stands out based on cost-effectiveness analysis.

## 1. Introduction

The depletion of finite fossil fuel resources and growing environmental concerns regarding carbon emissions, atmospheric impact, and public health have led to the urgent prioritization of sustainable, environmentally friendly, and clean energy sources [1]. Hydrogen, a clean energy carrier, plays a crucial role in the transition to clean, sustainable, and renewable energy systems [2]. Renewable energy systems that integrate hydrogen with electrochemical devices such as batteries and fuel cells can achieve high efficiency and zero carbon emissions, thereby accelerating the pace of energy transition [3]. However, the rapid and large-scale development of hydrogen energy in a short period is hindered by the limitations and complexity of infrastructure for its production, utilization, and storage [4]. Ammonia is a promising indirect hydrogen storage medium due to its high bulk hydrogen density, low storage pressure, and long-term storage stability [5–8], which enables on-line hydrogen production and multi-scenario utilization. Compared with conventional hydrogen production strategy by reforming of methane or methanol, ammonia is a cleaner hydrogen carrier and provides a closed-loop solution for the utilization of hydrogen energy from zero-carbon ammonia. Besides, ammonia effectively solves the problem of safety when storing and transporting hydrogen at high densities.

Meanwhile, distributed power generation based on fuel cell is being used on a large scale in residential, commercial and industrial applications [9–11]. Afif, Radenahmad [12] analyzed the ammonia-fed solid oxide fuel cell (SOFC), concluding that it is a promising next-generation energy source. Miyaoka, Miyaoka [13] studied the use of purified hydrogen from ammonia decomposition in PEMFCs for electricity generation, highlighting the potential use of ammonia in the future energy system. Cinti, Liso [14] proposed a high-temperature PEMFC system with ammonia decomposition, achieving a system energy efficiency of

This article is part of a special issue entitled: Hypothesis19(Basile) published in International Journal of Hydrogen Energy.

* Corresponding author.
** Corresponding author.
*E-mail addresses:* zcy_peace@hust.edu.cn (C. Zang), songli@hust.edu.cn (S. Li).

https://doi.org/10.1016/j.ijhydene.2025.01.480
Received 24 October 2024; Received in revised form 25 January 2025; Accepted 30 January 2025

**Nomenclature**

*Abbreviation*

| | |
|---|---|
| AD | Ammonia decomposer |
| PEMFC | Proton exchange membrane fuel cell |
| HS | Hydrogen storage device |
| ES | Electrical storage device |
| SOC | State of charge |

*Parameters*

| | |
|---|---|
| $k_f$ | Reaction rate constant |
| $R$ | Molar gas constant (J/mol·K) |
| $T$ | Thermodynamic temperature (K) |
| $W/F$ | Contact time between catalyst and feed gas ((g cat. h)/mol) |
| $E$ | Membrane effective factor |
| $\alpha$ | Pre-exponential factor |
| $V/E$ | Voltage (V) |
| $E_s$ | Separation activation energy (kJ/mol) |
| $\delta$ | Membrane thickness (μm) |
| $\xi_1/\xi_2/\xi_3/\xi_4$ | Empirical parameter |
| $C_{O2}$ | Concentration of oxygen |
| $A_{st}$ | Active area of PEMFC ($cm^2$) |
| $B$ | Stack coefficient |
| $N$ | Number of the cell |
| $\eta$ | Efficiency |
| $\mu$ | Valve opening |
| $\mu_{st}$ | Hydrogen utilization rate of fuel cell |
| $m$ | Mass flow (kg/h) |
| $C$ | Cost ($) |
| $k_v$ | Flow coefficient of the valve ($m^3$/h) |
| $E_a$ | Activation energy (J/mol) |
| $X$ | Dissociation rate |
| $F$ | Molar flow (mol/s) |
| $A$ | Area ($m^2$) |
| $p$ | Pressure (Pa) |
| $I$ | Current (A) |
| $F$ | Faraday constant (C/mol) |
| $i$ | Current density ($A/cm^2$) |
| $\lambda$ | Membrane resistor parameter |
| $l$ | Membrane thickness (mm) |
| $P$ | Power output (kW) |
| $C_{ap}$ | Battery capacity (kWh) |
| $R_{in}$ | Internal resistance |
| $\rho_N$ | Density ($kg/m^3$) |
| $T_{LP}$ | Lifespan of the system |

*Subscript*

| | |
|---|---|
| n | Partial pressure index |
| L | Low-pressure side |
| pur | Purge gas |
| st | Fuel cell stack |
| Li | Lithium-ion |
| maint | Maintenance |
| PV | Proportional valve |
| H | High-pressure side |
| imper | Impermeable gas |
| cell | Sigel cell |
| bat | Battery |
| cons | Consumption |
| OC | Open circuit voltage |

up to 40.1%. Meng, Cui [15] developed a liquid ammonia-fueled SOFC-PEMFC hybrid system with a thermoelectric efficiency of up to 95%. Duong, Ryu [16] integrated SOFC, PEMFC, gas turbine, and waste heat recovery systems, achieving an overall energy efficiency of 60.69% and exergy efficiency of 57.5%. Xu, Zhang [17] proposed a hybrid power generation system of PEMFC and combustion engine based on ammonia decomposition subsystem with maximum power of 16.23 kW and efficiency of 50.28%. Gong, Xu [18] compared ammonia- and methanol-fueled SOFC–CHP systems and found that the ammonia-fueled system exhibited higher electrical and overall efficiencies. Nie, Huang [19] simulated and compared ammonia-fueled power systems, including those using only internal combustion engines (ICE), only PEMFC and a combination of ICE and PEMFC. The PEMFC-based ammonia fuel system demonstrates optimal efficiency at lower power levels, with a maximum efficiency of up to 40.98%.

In general, the literature review indicates that utilizing ammonia as a fuel for fuel cells has the potential to enhance both the output power and overall efficiency of the system. Among different types of fuel cells, PEMFC stands out due to its faster response and higher efficiency. The ammonia-fueled fuel cell system boasts high energy density, low-cost storage and transportation, high safety, high efficiency, and low fuel cost [20,21]. Moreover, the presence of energy storage devices enhances the flexibility and reliability of energy supply. Compared with traditional fossil fuel systems, this system offers greater cost-effectiveness [22]. Consequently, an ammonia decomposer power generation system for PEMFC holds promise in improving efficiency and power generation. This integrated system can find applications in distributed power generation and energy storage, offering a potential solution to challenges such as energy shortage and global warming.

The integration of distributed power generation system into existing energy infrastructures necessitates the development of innovative energy management and distribution methodologies. Appropriate control strategies that can rapidly adapt to load fluctuations are essential. Peng, Zhao [23] proposed an energy management strategy which mainly based on state machine for the PEMFC, the results showed that the proposed strategy could achieve an increase in fuel efficiency of nearly 7% and optimal oxygen excess ratio operation of the PEMFC power subsystem. Wang, Li [24] analyzed an online identification power allocation method based on forgetting factor recursive least square (FFRLS) algorithm to minimize the hydrogen consumption of PEMFC system, which could achieve higher system efficiency(43.319%) and less system hydrogen consumption(3.821g). Fathy, Abdelkareem [25] analyzed a strategy based on the maximum power tracking method of PEMFC, which had the high reliability and efficiency. Yuan, Chen [26] examined the operating characteristics of the PEMFC-based CHP system in various strategies including constant-power output, electrical-led output, and stepped electrical-led output. The results indicated that the total system efficiency reaches 95.62% in the constant power output strategy. Cai, Wang [27] developed four strategies for data center applications using PEMFC, in which the complementary nature of different energy storage devices (thermal storage tanks and batteries) and multiple energy sources was taken into account. In addition, economic analysis is another key system evaluation criterion. Cesaro, Ives [28] predicted the cost of a large green ammonia power plant by examining ammonia fuel costs, equipment costs, and maintenance costs. Shahverdian, Sohani [29] conducted an economic evaluation of a photovoltaic wind power generation system with PEMEC-PEMFC based on techno-economics, which take the installation cost of each component of the system as well as profitability of the electricity sold into account.

Numerous scholars have conducted extensive thermodynamic modeling and analysis of ammonia-fueled PEMFC power systems, highlighting their significant advantages such as clean and efficient energy conversion capabilities [30–33]. These systems are recognized for their potential applications in transportation and distributed power

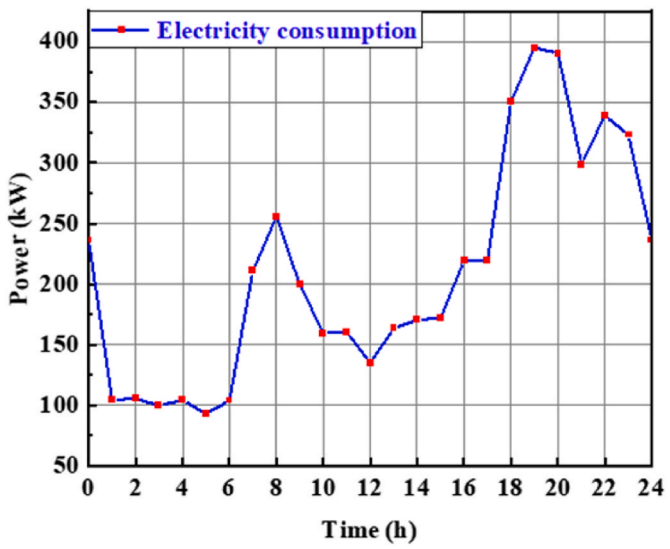


**Fig. 1.** Hourly electrical consumption curve of users of 285 individual household.

generation. However, previous studies have mainly focused on the regulation of hydrogen energy and the performance of the PEMFC in terms of power and efficiency. In the context of PEMFC systems with ammonia decomposed hydrogen for supply, the complexity and multi-coupled nature of ammonia-fueled systems necessitate the development of strategies that promote system stability, economic feasibility, and control flexibility. Major contributions of this study are summarized as follows.

(1) In order to provide a more accurate and comprehensive understanding of the system characteristics and control action, the performance of ammonia catalytic cracking-based PEMFC system including the ammonia decomposer, palladium membrane separator, PEMFC, hydrogen storage tanks, lithium battery and end-user components were assessed.
(2) This study proposes various strategies designed to improve the operation stability and regulation efficiency of PEMFC systems using ammonia catalytic decomposer. The findings provide new perspectives on the application of ammonia-catalyzed hydrogen production within PEMFC power generation systems.
(3) Comprehensive performance and tech-economic analysis of the system under the five control strategies from the perspectives of valve switching times, fuel cell status, average system efficiency and daily cost have been conducted.

## 2. System description

### 2.1. Electrical consumption

The residential electrical consumption curve is obtained from 285 households [34] as shown in Fig. 1. The curve exhibits two peaks, occurring in the morning and evening, with the highest load reaching 398 kW at 19:00. The daily electricity demand fluctuates within the range of 98–398 kW. This study focuses on ammonia feed in different operating modes, including hourly-flow input mode, stepped-flow input mode and constant-flow input mode using the strategies described in Section 2.2 assuming that the hourly electrical consumed by the user remains constant.

### 2.2. System diagram and control strategy

The proton exchange membrane fuel cell-based power system, fueled

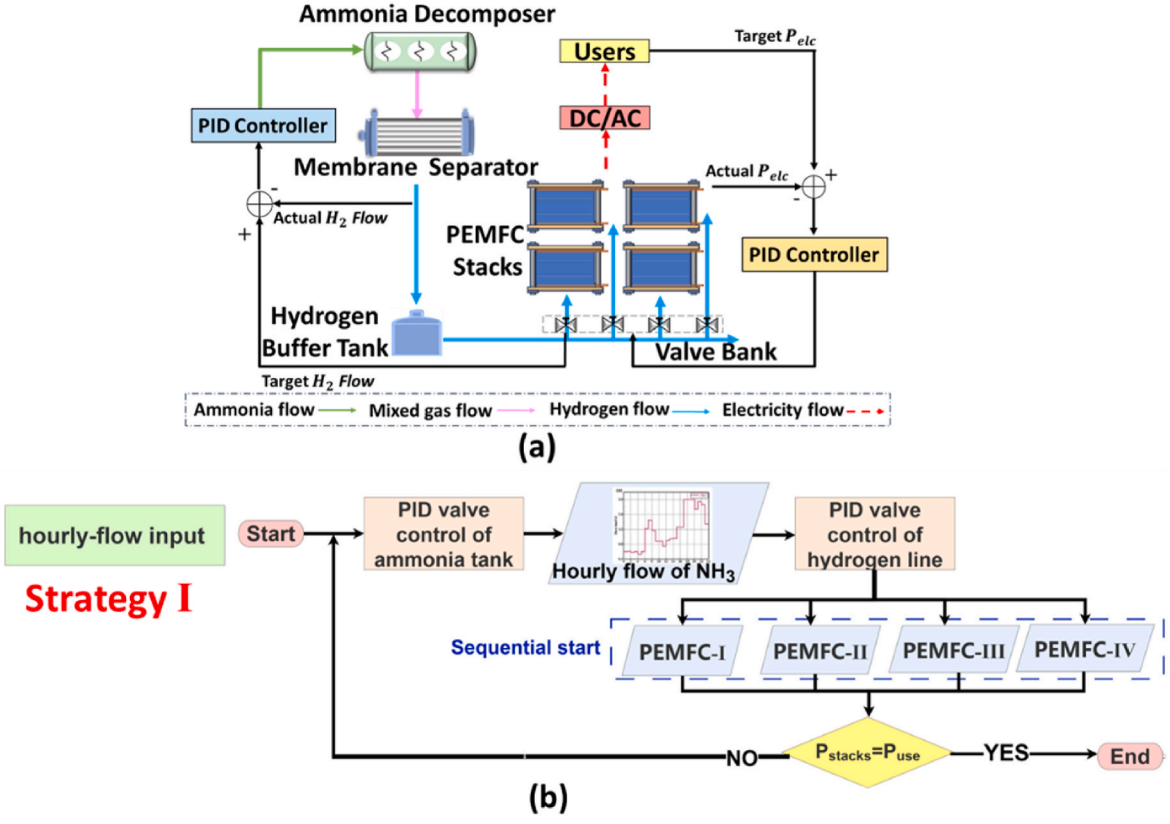


**Fig. 2.** Schematic diagram of the system and the corresponding control strategy: (a) AD-PEMFC, (b) Strategy I for hourly control.

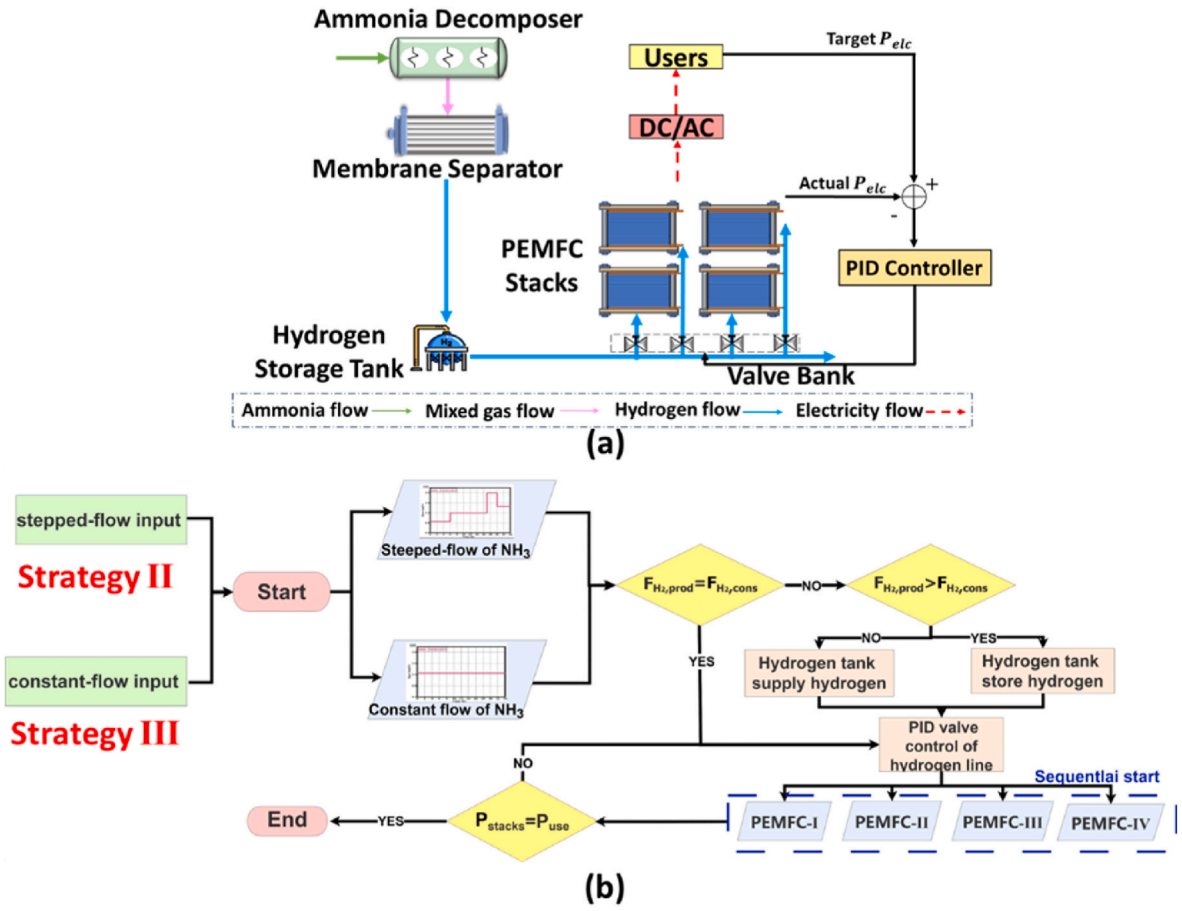


**Fig. 3.** Schematic diagram of the system and the corresponding control strategy: (a) AD-PEMFC-HS, (b) Strategy II for stepped flow and III for constant flow.

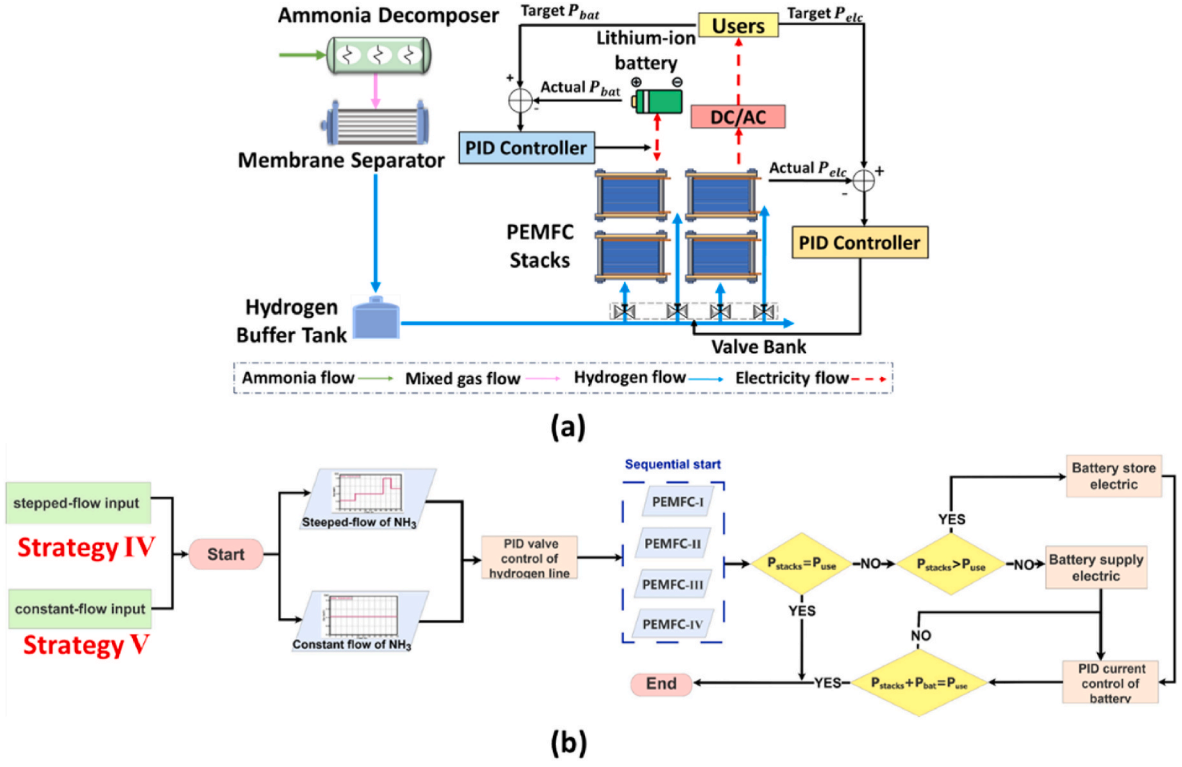


**Fig. 4.** Schematic diagram of the system and the corresponding control strategy: (a) AD-PEMFC-ES, (b) Strategy IV for stepped flow and V for constant flow.

**Table 1**
Values of kinetic parameters of the ammonia decomposer [41].

| | Value | Unit |
|---|---|---|
| $k_0$ | 7.54e+10 | kmol/m$^3$·s |
| $E_a$ | 219 | kJ/mol |

by hydrogen derived from ammonia decomposition, is employed to meet load demands through the coordinated control of the fuel cell, hydrogen storage tanks, and lithium batteries. The system configuration and control strategies are presented in the following sections.

PEMFC system based on ammonia decomposition (AD-PEMFC) is shown in Fig. 2a, including ammonia decomposer, membrane separator and PEMFC. An energy storage device is considered as an auxiliary control. The ammonia decomposer has a hydrogen production capacity of 250 Nm$^3$/h [35]. Ammonia undergoes catalytic decomposition into nitrogen and hydrogen at a maintained reaction temperature of 873K to ensure complete decomposition [36]. Following the catalytic decomposition, the resulting gas mixture proceeds into a palladium membrane separator, facilitating the final stage of hydrogen separation and purification, ultimately achieving a purity level of 99.99%. The high-purity hydrogen received by the buffer tank flows through the valve manifold into the four fuel cell stacks with a maximum power of 100 kW each, where it undergoes electrochemical reactions. As shown in Fig. 2b, Strategy I (Hourly AD-PEMFC) adjust the ammonia feed hourly using a PID controller to produce the required amount of hydrogen for the power system. If the electrical demand exceeds the maximum power output of the current fuel cell stack $i$ ($i = 1, 2, 3$), the hydrogen valve of the next fuel cell stack ($i + 1$) is gradually opened for additional electricity generation. If the electrical demand is between the maximum power output of the previous fuel cell stack ($i$ - 1) and the current fuel cell stack ($i$), the opening of the hydrogen valves of the current fuel cell stack ($i$) is adjusted in the range 0–1 so that it matches the electrical demand. Following this, the output power is converted by a converter before being sent to the user. Notably, the hydrogen is produced and utilized immediately, with no energy storage implemented in this system.

Fig. 3a shows the AD-PEMFC system with hydrogen storage device (AD-PEMFC-HS). The system incorporates a high-pressure hydrogen storage tank of 350 bar [37] as its energy storage device. Hydrogen from the outlet of the membrane separator is stored in the tank, and the fuel cell power output is modulated according to user requirements by controlling the opening of the valve bank. Based on the hourly electrical consumption curve of Fig. 1, electrical power can be divided into four stages: 0:00–5:00, 5:00–17:00, 17:00–20:00, and 20:00–24:00. Ammonia is decomposed into hydrogen to generate electricity in PEMFC, so four ammonia flow rates (0.85, 1.2, 1.5, and 2 mol/s) corresponding to the average electric power of four stages can be derived. As shown in Fig. 3b, Strategy II (Stepped AD-PEMFC-HS) varies the ammonia feed rate in four steps. If the amount of pure hydrogen produced exceeds the amount consumed for power generation, the excess is stored in the hydrogen storage tank, conversely, if the amount of pure hydrogen produced is less than the amount consumed, the shortfall is supplied by the hydrogen storage tank. Strategy III (Constant AD-PEMFC-HS) involves feeding ammonia at a constant flow rate of 1.2575 mol/s which is obtained by averaging the electric power consumption, using a high-pressure hydrogen storage tank. The remaining regulations are identical to those in Strategy II.

Fig. 4a shows the AD-PEMFC system with electrical storage device (AD-PEMFC-ES) using a lithium-ion battery. In this system, the hydrogen from the outlet of the membrane separator enters the buffer tank before flowing into the fuel cell stack through the valve bank. The power generation of the system is finely regulated to meet user needs through coordination between the fuel cell and the lithium-ion battery. As shown in Fig. 4b, Strategy IV (Stepped AD-PEMFC-ES) involves stepwise changes in the ammonia feed and uses a lithium-ion battery as the energy storage device. The resulting pure hydrogen is fully fed into the fuel cell stacks. By co-regulating the hydrogen line valve of the fuel cell and the current of the battery, the power generation of the system is regulated to match the electrical consumption. In Strategy V (Constant AD-PEMFC-ES), ammonia is supplied at a constant flow rate of 1.2575 mol/s, along with a lithium-ion battery. The remaining regulations are identical to those in Strategy IV.

## 3. Mathematical model

The model of an integrated fuel cell system based on ammonia catalytic cracking is established including the ammonia decomposer, membrane separator, PEMFC, lithium-ion battery for energy storage and proportional valve to regulate the hydrogen flow rate. Different strategies for controlling the system were then applied and an economic evaluation model developed to assess the system of each strategy. In this section, the modeling process was thoroughly elucidated. The models were constructed using Simulink, incorporating various essential blocks such as Signal Builder, MATLAB Function, and PID Controller. Additionally, basic arithmetic operation blocks (e.g., addition, subtraction, multiplication, and division) were employed to facilitate the necessary calculations. The simulation settings include a maximum step size of 1 s to ensure accurate and stable results.

### 3.1. Ammonia decomposer (AD)

Ammonia cracking reaction formula of ammonia reforming for hydrogen production is [38]:

$$NH_3 \rightleftharpoons 1.5H_2 + 0.5N_2 \tag{1}$$

Ammonia decomposition is a heat-absorbing process, with an enthalpy of 11 kcal mol$^{-1}$ [39]. At temperature above 623 K, the equilibrium conversion is close to 100%. The rate constant of ammonia cracking reaction is in accordance with the law of Arrhenius and can be expressed as follows [40] (see Table 1) :

$$k_f = k_0 \exp\left(\frac{-E_a}{RT_{AD}}\right) \tag{2}$$

where $k_f$ is the ammonia catalytic rate constant of reaction, $k_0$ is a parameter, $E_a$ is the activation energy, $T_{AD}$ is the decomposition temperature.

Ammonia degradation rate depends on both the contact time between catalyst and feed gas and temperature. Ammonia degradation rate can be calculated from literature [41]:

$$1 - X_{NH_3} = \exp\left(-k_f(W/F)\right) \tag{3}$$

where $X_{NH3}$ is the ammonia dissociation rate, $W/F$ is the contact time between catalyst and feed gas, $W$ is the weight of the catalyst, $F$ is the ammonia flow rate.

The hydrogen flux for catalytic cracking of ammonia can be obtained from Equation (4):

$$F_{H_2,AD} = F_{NH_3} X_{NH_3} \tag{4}$$

### 3.2. Membrane separator (MS)

The hydrogen purity of 99.99% is required for PEMFC, thus the separation and purification of the gas mixture from the ammonia cracker is indispensable. Palladium membrane separators with the advantages of high hydrogen purity, permeability and low temperature operation [42] is commonly adopted. Hydrogen permeation across the palladium membrane is achieved using a partial pressure difference, and the hydrogen separation flux is calculated by the hydrogen permeation equation [43]:

**Table 2**
Key parameters of PEMFC stack.

| Variables | Symbol | Values |
|---|---|---|
| Operating pressure | $P_{H2}/P_{O2}$ | 3 atm/3 atm |
| Working temperature | $T_{st}$ | 353 K |
| Empirical parameter | $\xi_1/\xi_2/\xi_3/\xi_4$ | -0.9514/0.00312/0.000074/-0.000187 |
| Active area | $A_{st}$ | 287 $cm^2$ |
| Membrane thickness | $l$ | 0.051 mm |
| Membrane water content | $\lambda$ | 14 |
| Stack coefficient | $B$ | 0.016 |
| Number of unit cell | $N$ | 480 |

$$F_{H_2,MS} = \varepsilon \frac{A_{MS}}{\delta_{MS}} \alpha \, exp\left( -\frac{E_s}{RT_{MS}} \right) \left( p_H^n - p_L^n \right) \tag{5}$$

where $F_{H_2,MS}$ is the hydrogen mass flow rate from MS, $\varepsilon$ is the membrane effective factor, $A_{MS}$ is the membrane area, $\alpha$ is the pre-exponential factor, $E_s$ is the separation activation energy, $T_{MS}$ is the separator temperature, $p$ is the partial pressure of $H_2$ ($H$ and $L$ represent the high-pressure and low-pressure side, respectively), $\delta_{MS}$ is the membrane thickness, and $n$ is the partial pressure index($n = 0.5$).

To increase the amount of pure hydrogen at the outlet of the palladium membrane separator, a purge gas is used on the low-pressure side of the membrane. The high-pressure inlet side and the low-pressure outlet side of the gas are in a state of flat push flow, with the gas flowing in the same direction on both sides. In this flow model, an infinitesimal palladium membrane capacity $dx$ the hydrogen permeated can be expressed as [44]:

$$dF_{H_{2,MS}dx} = C\left[ \left( \frac{F_{H_{2,AD}} - F_{H_{2,MS}dx}}{F_{imper} + F_{H_{2,AD}} - F_{H_{2,MS}dx}} p_H \right)^{0.5} - \left( \frac{F_{H_{2,MS}dx}}{F_{pur} + F_{H_{2,MS}dx}} p_L \right)^{0.5} \right]^{-1} dx \tag{6}$$

where $dF_{H_{2,MS}dx}$ is the hydrodynamic separation mass flow rate at infinitesimal points, $F_{imper}$ is the gas flow rate without passing through palladium membrane, $F_{pur}$ is purge gas flow rate on the separation side, $C = \varepsilon\alpha \exp\left( -\frac{E_s}{RT_{MS}} \right)$.

### 3.3. PEMFC

The fuel cell stacks in this study are identically configured with a maximum electrical power output of 100 kW with parameters in Table 2. The voltage output of the fuel cell unit is lower than the theoretical open-circuit voltage due to the activation voltage, the ohmic voltage and the concentration voltage. The voltage and energy balance of the PEMFC stacks are expressed as follows [45]:

$$V_{cell} = E_{Nernst} - V_{act} - V_{ohm} - V_{conc} \tag{7}$$

where $V_{cell}$ is the cell voltage, $E_{Nernst}$ is the open-circuit voltage, $V_{act}$ is the activation voltage loss, $V_{ohm}$ is the ohmic voltage loss, $V_{conc}$ is the concentration voltage loss.

The open-circuit voltage is [46]:

$$E_{Nernst} = 1.229 - 8.5 \times 10^{-4}(T_{st} - 298.15) + \frac{RT_{st}}{2F} ln\left( p_{H_2} \times p_{O_2}^{0.5} \right) \tag{8}$$

where $T_{st}$ is the PEMFC stack temperature, and $P_{H2}$ ($P_{O2}$) represents the pressure of hydrogen (oxygen).

Activation voltage loss is:

$$V_{act} = \xi_1 + \xi_2 T_{st} + \xi_3 \, ln(C_{o_2}) + \xi_4 T_{st} \, ln(I) \tag{9}$$

$$C_{O_2} = \frac{P_{O_2}}{5.08 \times 10^6 \exp\left( \frac{-498}{T_{st}} \right)} \tag{10}$$

where $\xi_i$ (i = 1–4) is an empirical parameter, $I$ is the working current of the stack.

Ohmic voltage loss is:

$$V_{ohm} = IR_{ohm} \tag{11}$$

$$R_{ohm} = \frac{181.6\left[ 1 + 0.03i + 0.0062\left( \frac{T_{st}}{303} \right)^2 i^{2.5} \right]}{\left[ \lambda - 0.634 - 3i \times \exp\left( 4.18\left( \frac{T_{st}-303}{T_{st}} \right) \right) \right]} \times \frac{l}{A_{st}} \tag{12}$$

where $i$ is the current density, $\lambda$ is the membrane water content, $l$ is the thickness of the proton exchange membrane, $A_{st}$ is the active area of PEMFC.

Concentration voltage loss is:

$$V_{conc} = -B \ln\left( 1 - \frac{i}{i_{\max}} \right) \tag{13}$$

where $B$ is the stack coefficient, $i_{max}$ is the maximum current density.

With these voltages determined, the output power of the PEMFC can be calculated:

$$P_{st} = NV_{cell}I \tag{14}$$

where $N$ is the number of fuel cells.

The hydrogen consumption during the electrochemical reaction can be calculated as follow:

$$F_{H_{2,cons}} = \frac{NI}{2F}\mu_{st} \tag{15}$$

where $\mu_{st}$ is the hydrogen utilization rate of fuel cell.

### 3.4. Lithium-ion battery

State of charge (SOC) is a key indicator of how a battery operates and represents the percentage of available battery power compared to its maximum power. The current is integrated to obtain the state of charge of a Li-ion battery [47]:

$$SOC(t) = SOC(t_0) + \frac{\eta_{bat}}{C_{ap}} \int_{t_0}^{t} I_{Li}(t)dt \tag{16}$$

where $SOC(t_0)$ is the initial value of the $SOC$, $C_{ap}$ is the battery capacity, $\eta_{bat}$ is the coulombic efficiency, and $I_{Li}$ is the working current of the lithium-ion battery. Negative and positive values of $I_{Li}$ indicate that the battery is in the charge and discharge states, respectively.

The operating voltage of the lithium battery is calculated from the open circuit voltage and internal resistance:

$$V_{bat} = V_{OC} - R_{in}I_{Li} \tag{17}$$

where $V_{bat}$ is the lithium-ion battery operating voltage, $V_{OC}$ is the open circuit voltage, $R_{in}$ is cell resistance, $I_{Li}$ is the operating current of lithium-ion battery.

The open circuit voltage and internal resistance are related to the SOC, and the specific parameters can be taken according to the test, and the calculation formula is as follows [48]:

$$V_{OC} = -1.031e^{-35SOC} + 3.685 + 0.2165SOC - 0.1178SOC^2 + 0.3201SOC^3 \tag{18}$$

$$R_{in} = 0.1562e^{-24.37SOC} + 0.07446 \tag{19}$$

The output power of a lithium battery can be obtained from the current voltage:

$$P_{bat} = V_{bat}I_{Li} \tag{20}$$

**Table 3**
Economic parameters used for the system.

| Cost source | Value |
|---|---|
| AD [51] | 1.96$/Nm$^3$h$^{-1}$ |
| MS [52] | 746$/m$^2$ |
| PEMFC [53] | 600$/kW |
| Lithium-ion battery [53] | 33$/kWh |
| Hydrogen storage tank [54] | 500$/kg |
| Ammonia [17] | 1$/kg |
| Hydrogen [55] | 7.61$/kg |
| Electricity [53] | 0.078$/kWh |
| Annual maintenance [56] | 5% of the initial investment |

### 3.5. Proportional valve

To control the pressure and flow of hydrogen into the fuel cell, a proportional valve is required. The flow through the valve body can be expressed as [49]:

$$m_{PV,out} = \mu m_{PV,max} \tag{21}$$

where $m_{PV,out}$ is the hydrogen mass flow at valve outlet, $\mu$ is the control signal of valve opening with the range of 0–1, $m_{PV,max}$ is the maximum mass flow that the valve can flow through.

The valve body's maximum flow rate is calculated based on its low and high flow rate pressure drops when $P_{out}$>0.528$P_{in}$ [50]:

$$m_{PV,\max} = 1.27 \times 10^{-7} \times k_v \sqrt{\frac{p_{out}(p_{out} - p_{in})}{T_{in}\rho_N}} \tag{22}$$

where $k_v$ is the flow coefficient of the valve body, $p_{in}$ and $p_{out}$ are the inlet and outlet pressure of the valve body, respectively. $T_{in}$ is the temperature of the inlet gas of the valve body, $\rho_N$ is the standard density of the gas flowing through the valve body.

### 3.6. Economic evaluation model

The economic evaluation of the system includes equipment investment costs, fuel costs, maintenance costs, and profitable revenues as described in Table 3. The ammonia flow rate and the different equipment states, which are reflected in the ammonia cracker, palladium membrane separator and energy storage, are the main differences in the economic evaluation of the different control strategies. In this study, the profitable revenues include electricity revenue and hydrogen revenue calculated using the grid price and pure hydrogen price. The index of evaluating the economic performance of the system and can be calculated as follows:

$$C_{average} = \frac{C_{equipment}}{365 \times T_{LP}} + \frac{C_{maint}}{365} + C_{NH_3} - C_{benefit} \tag{23}$$

where $C_{euipment}$ is the initial investment of equipment cost, $C_{maint}$ is the annual maintenance cost, $C_{NH3}$ is the fuel cost of ammonia, $C_{benefit}$ is profitable revenues, including electrical revenues as well as sales from electricity generated by stored battery or hydrogen. $T_{LP}$ is the lifespan of the system.

### 3.7. Performance assessment

To evaluate the system performance, two methods of calculating efficiency are proposed. The first one is the electrical efficiency of PEMFC:

$$\eta_{PEMFC} = \frac{P_{\text{PEMFC}}}{F_{H_2} LHV_{H_2}} \tag{24}$$

The electrical efficiency of distributed power system is defined as follows:

$$\eta_{\text{system}} = \frac{P_{\text{use}}}{F_{NH_3} LHV_{NH_3}} \tag{25}$$

where $F_{H_2}$ and $F_{NH_3}$ represent the molar flow of hydrogen for PEMFC consumed and ammonia for system consumed, $LHV_{H_2}$ and $LHV_{NH_3}$ represents the lower heating value of hydrogen and ammonia, $P_{\text{PEMFC}}$ and $P_{\text{use}}$ represent PEMFC power generation and power supplied by the system to the user, respectively.

## 4. Results and discussions

### 4.1. Model validation

The model of ammonia decomposer has been validated in previous study [57]. The membrane separator model is validated in Fig. 5a by comparing the predicted and measured hydrogen permeation capacity of the membranes at four pressures. An average relative error of 5.47% indicates the reliability of membrane separator model [58]. Fig. 5b shows the validation results of the PEMFC model with an average relative error of 2.61% [59]. Such deviations may result from is the empirical parameter of the model and the measurement error in the experimental test. Both comparisons are within the acceptable range, which is an indication of a good fit of the construction model.

### 4.2. System performance in different control strategies

(1) Strategy I: Hourly AD-PEMFC

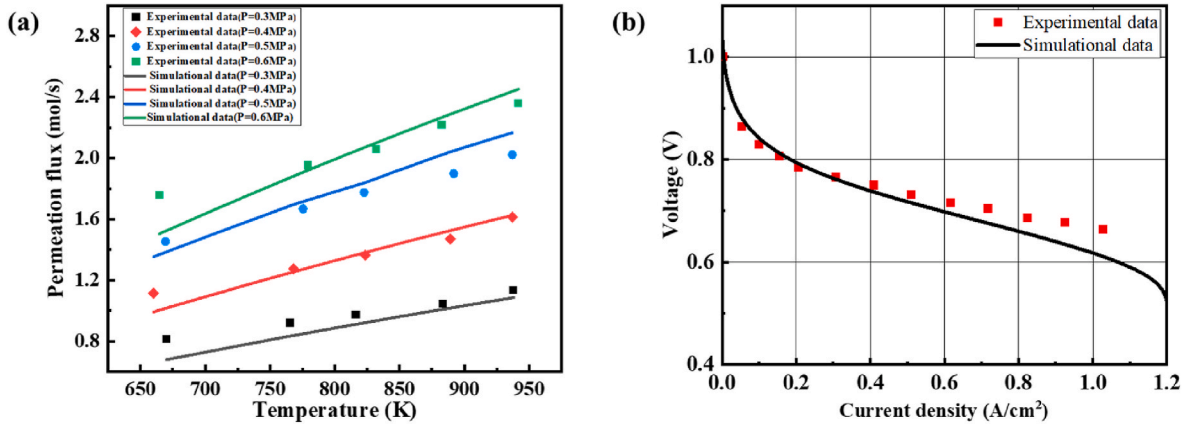


**Fig. 5.** Model validation for (a) Pd membrane separator and (b) PEMFC.

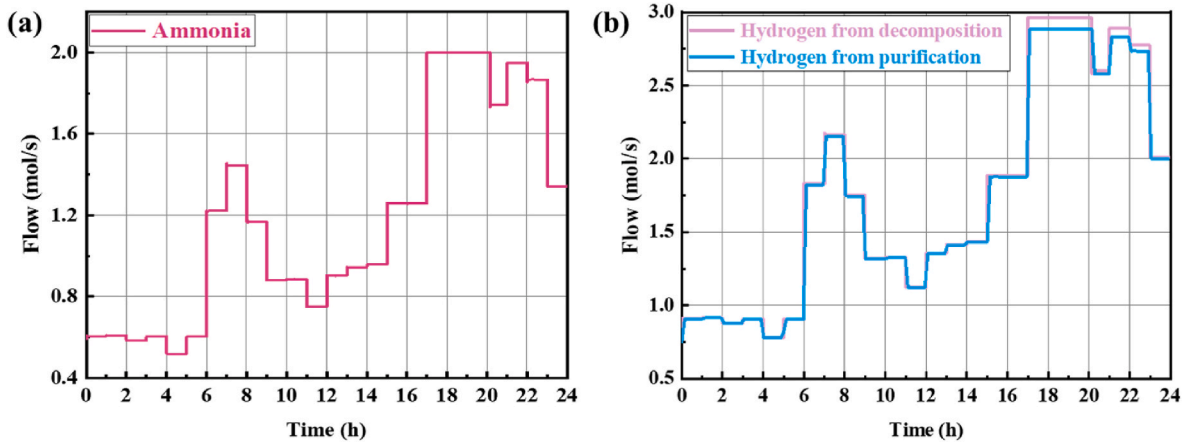


**Fig. 6.** Molar flow (a) Ammonia for AD, (b) Hydrogen production from decomposition and purification.

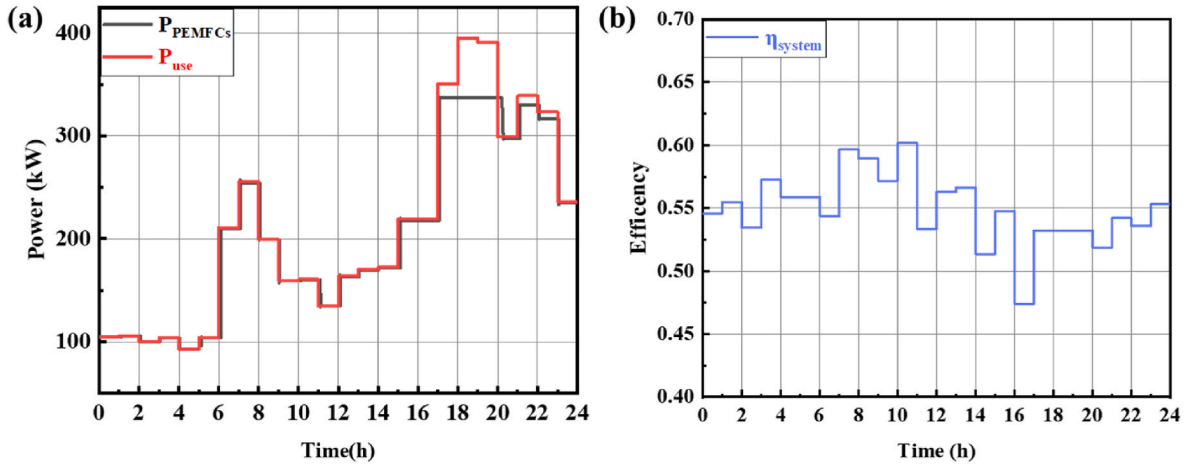


**Fig. 7.** (a) Power of PEMFC stacks and users, (b) Efficiency of system.

In Strategy I, the ammonia flow is adjusted hourly to match the electrical demand. The performance of the ammonia decomposer is shown in Fig. 6. Fig. 6a shows that the PID controller effectively regulates the ammonia feed with a decomposition rate of over 98%. However, the maximum generated hydrogen by the ammonia decomposer is not sufficient to meet the theoretical hydrogen consumption of the PEMFC (3.36 mol/s or 270.95 $Nm^3$/h) at maximum power consumption of 398 kW. As shown in Fig. 6b, the hydrogen flow at the outlet of the ammonia decomposer is low, so that the separation efficiency is close to 100%. But during the night peak period when hydrogen production is increasing, the hydrogen permeation of the separation unit is decreasing, so that the hysteresis between the pure hydrogen outlet of the palladium membrane and the mixed hydrogen outlet of the cracking unit become evident.

The total electricity from the fuel cell stacks and the electricity demand required by the users (Fig. 7a) indicates there is an energy gap due to the limited hydrogen production capacity of the ammonia decomposer during the night peak from 17:00 to 20:00, which corresponds to Fig. 6a. However, with the augmented production of hydrogen in the ammonia cracker, the burden of purifying the hydrogen escalates, consequently diminishing the efficiency of hydrogen separation. Despite the higher volume of hydrogen produced, the gain in pure hydrogen yield remains insignificant, leading to hydrogen wastage and an escalation in operational costs, which is less economically viable to meet the present electricity demand. The average system efficiency of such a strategy is approximately 54%, which is the highest among all strategies owing to the fact that all ammonia decomposed hydrogen was utilized for electricity generation (Fig. 7b).

Fig. 8a displays the power contribution of the four fuel cell stacks. Stack I maintains almost constant full power throughout the day, except during the period from 4:00 to 5:00 when the total power demand is lowest of about 93 kW. Stack II experiences the most frequent power variation throughout the day, varying by about 5 kW during the period from 0:00 to 6:00, due to the lowest user power consumption of about 105 kW. Stack II operates at full power during the first peak power consumption period from 6:00 to 9:00 a.m. In the following periods, the power of the stack fluctuates mainly in the range of 40–100 kW. Stack III is only activated during the first and second peaks, while Stack IV is only activated during the evening peak. Fig. 8b illustrates the efficiency variation of each power stack. Stack I maintains a stable efficiency of about 44%, while the efficiency of the other fuel cell stacks fluctuates with the power. As the fuel cell power increases, the electrical efficiency monotonically decreases, and the lowest electrical power is 44.25% at full power operation. The average electrical efficiencies of the four stacks are 44.33%,45.29%, 23.06%, and 14.03%, respectively (Fig. 8c). Stack I operates at full power for a long period of time, while stack II spends a longer period of time in the high efficiency zone, resulting in a higher average efficiency. Stack III and IV are not in operation for most time, resulting in the lowest average efficiency. The variation times of hydrogen valve for each stack (Fig. 8d) demonstrates that stack I requires the least times of valve switches, indicating a more stable operation. Whereas stack II experiences the most frequent valve switches due to power fluctuations in the range of 100–200 kW. Stack III and IV are mainly used during peak power consumption, resulting in a moderate

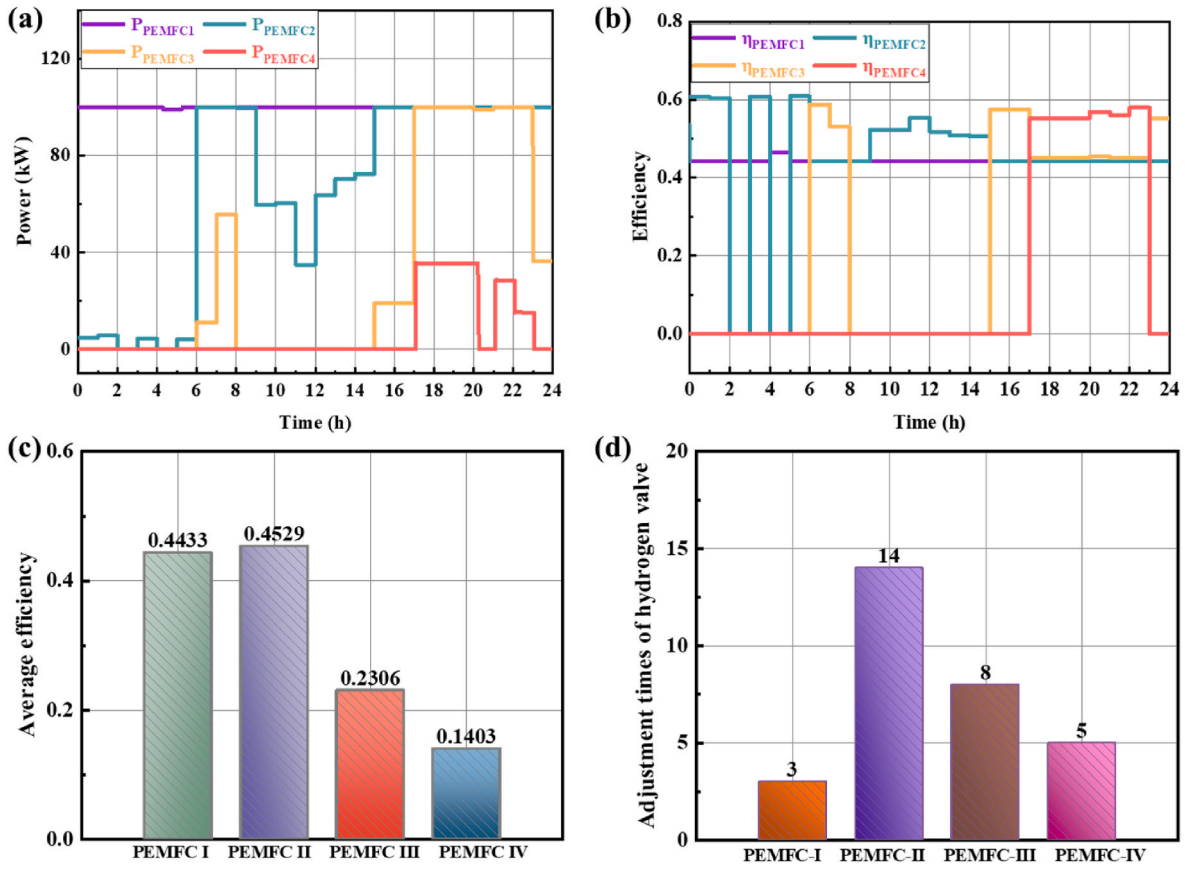


**Fig. 8.** Operating characteristics of the each PEMFC stack (a) Power, (b) Electrical efficiency, (c) Average efficiency, (d) Adjustment times of hydrogen valve.

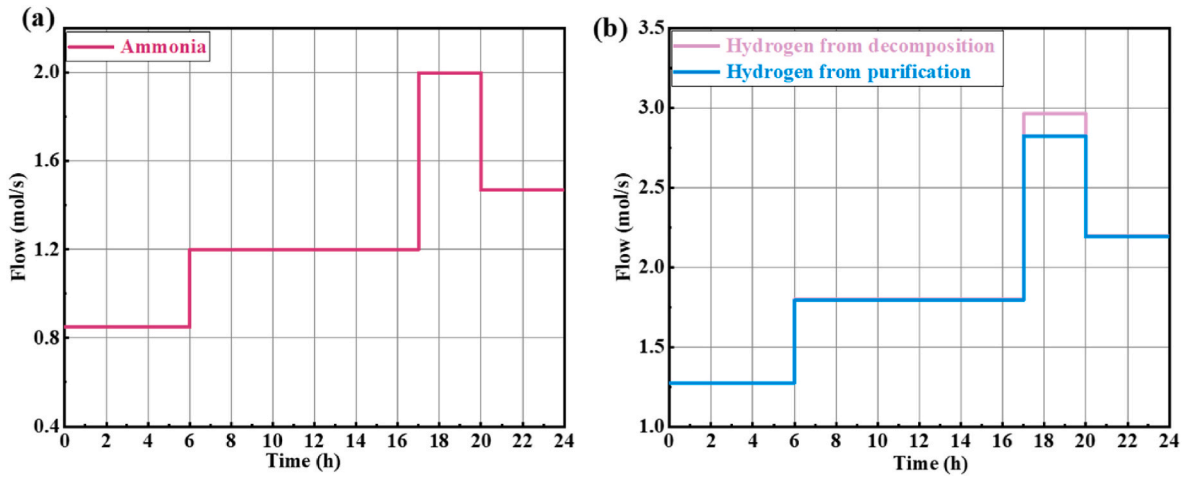


**Fig. 9.** Molar flow (a) Ammonia for AD, (b) Hydrogen production from decomposition and purification.

and similar frequency of valve switches.

(2) Strategy II: Stepped AD-PEMFC-HS

The main issue with Strategy I is the frequent adjustments in the operating state of the ammonia decomposer and the presence of poor matching. To overcome these drawbacks, Strategy II introduces a stepped input of ammonia flow, utilizing a hydrogen storage tank for power storage. The ammonia flow rate was consistently kept at four constant rates (0.85, 1.2, 1.5, and 2 mol/s), which was derived according to the four stages of hourly electrical consumption curves as mentioned in Section 2.2. The resulting hydrogen was stored in high-pressure tanks and adjusted in response to the power demand (Fig. 9a). The membrane separator performs consistently over time (Fig. 9b) with hydrogen separation rates of 95.34%–99.6%. The discrepancy in hydrogen flow rate between the palladium membrane outlet and the separator outlet is still present but reduced compared with Strategy I.

It is also revealed that the states of fuel cell stacks I, II and III are identical to Strategy I. Although ammonia is used for the gradual production of hydrogen, pure hydrogen is stored in high-pressure tanks and electricity is generated through a regulated valve bank. It is worth noting that the electrical efficiency decreases monotonically with

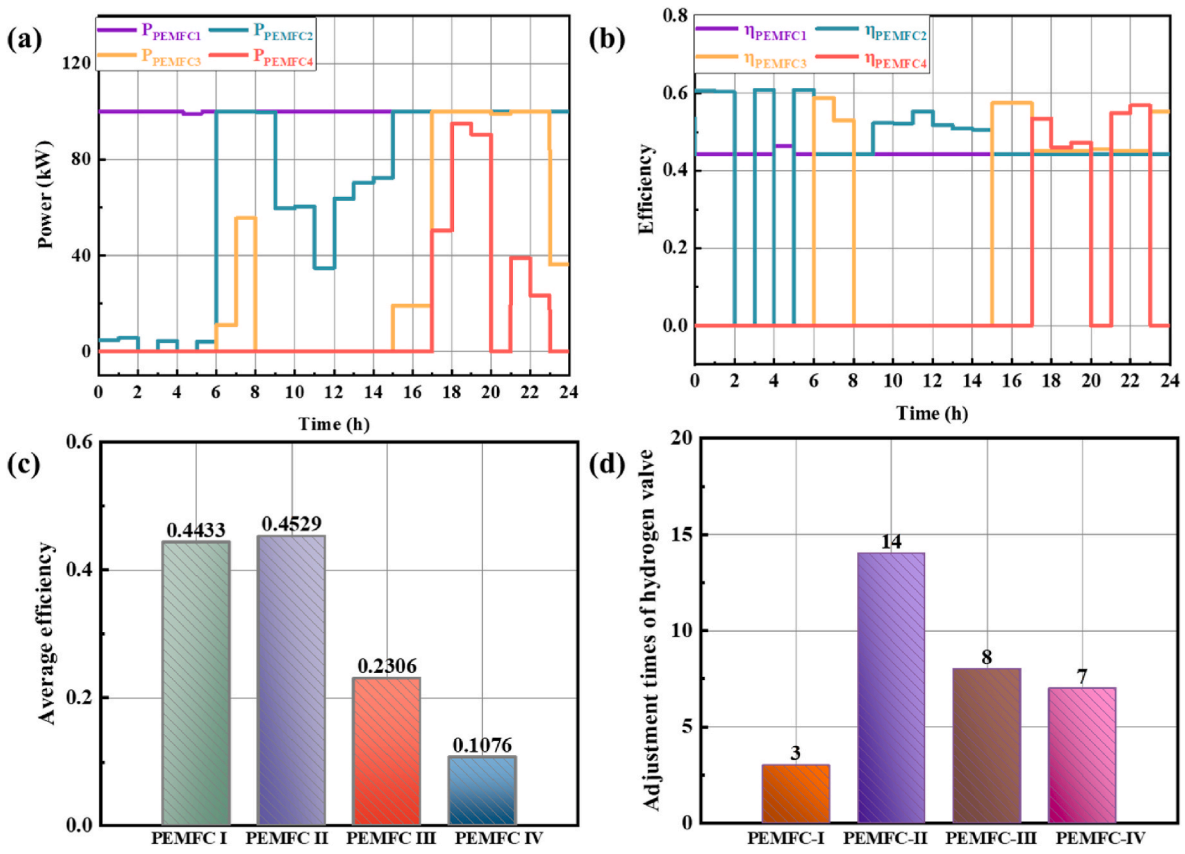


**Fig. 10.** Operating characteristics of the each PEMFC stack (a) Power, (b) Electrical efficiency, (c) Average efficiency, (d)Adjustment times of hydrogen valve.

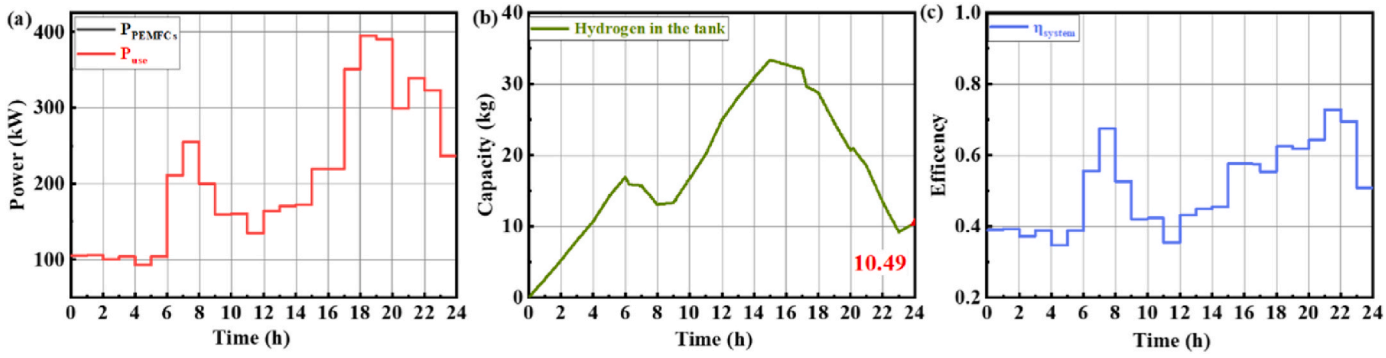


**Fig. 11.** (a) Power of PEMFC Stacks and user, (b) Mass of hydrogen in tank, (c) Efficiency of system.

power, resulting in stack IV generating more power compared to Strategy I with an average efficiency of 10.76% (Fig. 10a–c). In Strategy I, hydrogen production remains constant during peak hours (16:00–20:00) because the ammonia decomposer reaches its maximum production limit. As a result, PEMFC-IV cannot meet the power demand by adjusting the hydrogen valve. Therefore, compared to Strategy I, Strategy II requires increased adjustment times of the hydrogen valve for Stack IV (Fig. 10d).

In Strategy II, the power generated by the fuel cell stacks perfectly matches the electrical demand (Fig. 11a). The hydrogen storage capacity in tanks increases when hydrogen production exceeds hydrogen consumption and decreases when hydrogen production is lower than consumption (Fig. 11b). The hydrogen supply from the hydrogen storage tanks is highest between 6:00–8:00 and 17:00–20:00, corresponding to the highest power demand. During the all-day operation, 10.49 kg hydrogen is stored. The system efficiency ranged from 34.65% to 77.92% (Fig. 11c). During hydrogen storage, the ammonia-derived hydrogen did not fully convert into electricity, resulting in lower system efficiency. However, when hydrogen was supplied from storage tanks, the ammonia-derived hydrogen was fully utilized for electricity generation, leading to higher system efficiency.

(3) Strategy III: Constant AD-PEMFC-HS

Unlike Strategies I and II, Strategy III employed a consistent ammonia flow rate of 1.2575 mol/s into the decomposer, along with a constant rate of hydrogen flow (Fig. 12a). This approach was chosen to maintain system operation stability and prevent efficiency reduction caused by frequent adjustments. The working conditions of the ammonia decomposer remain constant with the conversion rate of 99.9%, and both the hydrogen purification and separation rate is 99.68%(Fig. 12b), due to the reduction of the feed ammonia flow rate

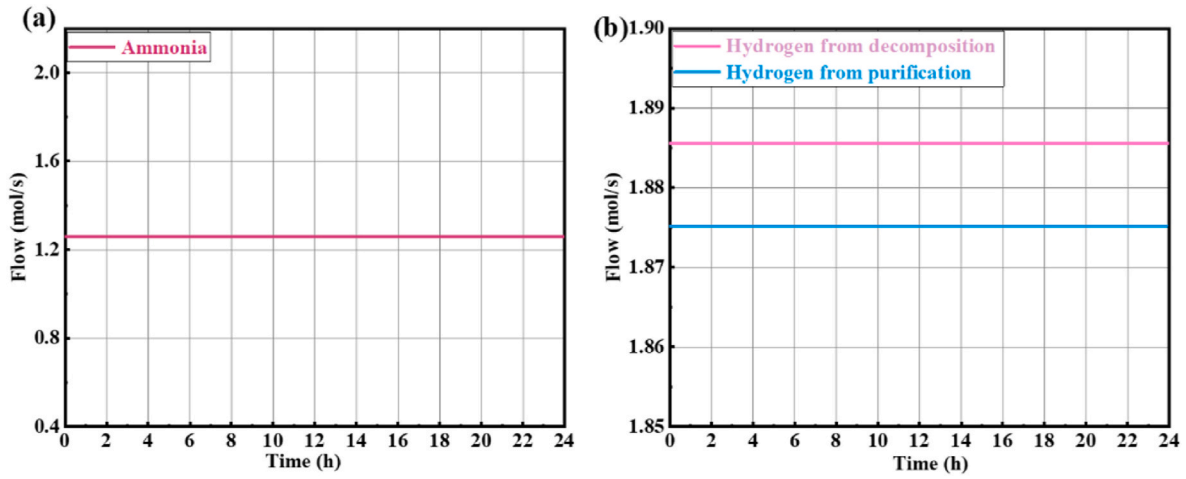


**Fig. 12.** Molar flow (a) Ammonia for AD, (b) Hydrogen production from decomposition and purification.

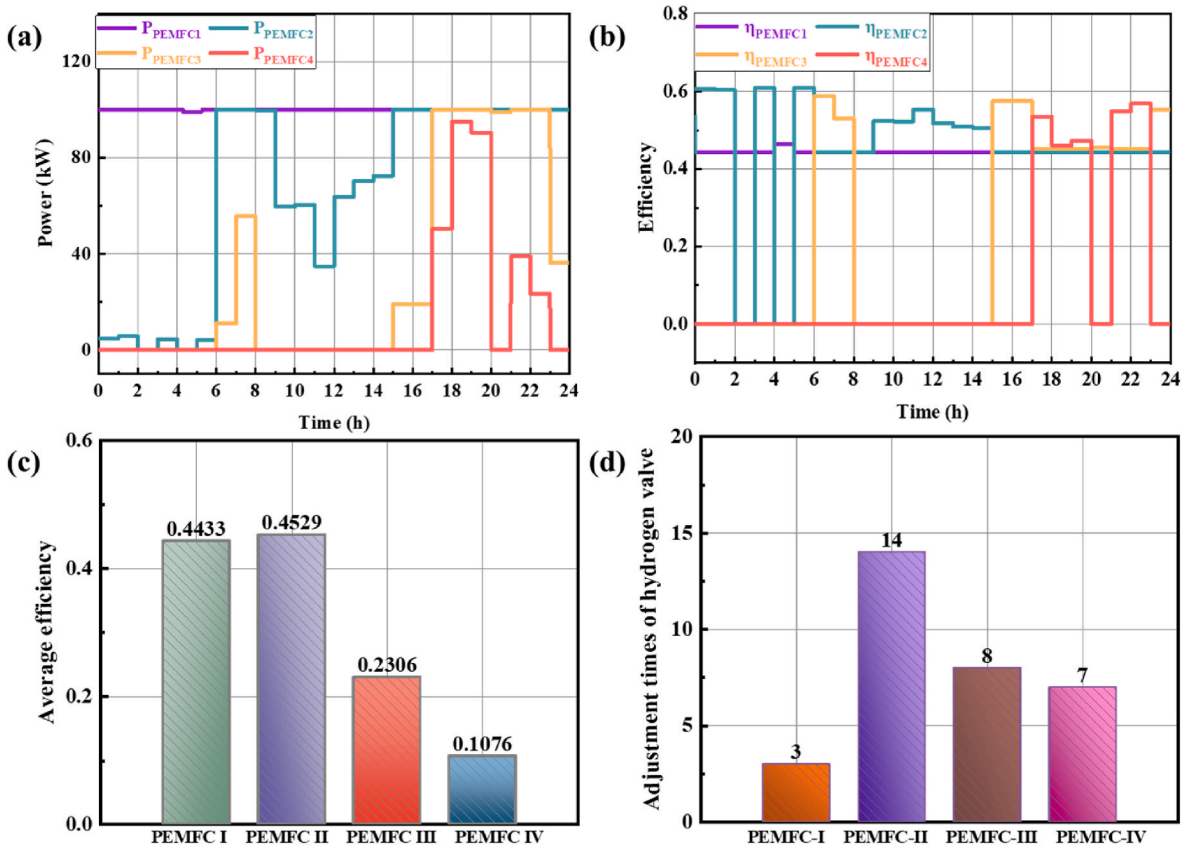


**Fig. 13.** Operating characteristics of the each PEMFC stack (a) Power, (b) Electrical efficiency, (c) Average efficiency, (d) Adjustment times of hydrogen valve.

and the higher W/F value. In constant flow operation, the front-end hydrogen production process is more stable and more favorable for decomposition and separation.

Strategy III uses the hydrogen storage tank as an energy storage device and adjusts the hydrogen valve according to user demand. The fuel cell stack states are identical to that of Strategy II (Fig. 13a–d). In the constant flow strategy, the power generated by the PEMFC stacks matches the electricity demand due to the co-regulation of the storage tanks (Fig. 14a). Fig. 14b shows that the ammonia conversion rate and hydrogen separation rate are higher due to the more stable front-end reaction process with 15.81 kg hydrogen stored, which is 5.32 kg greater than that of Strategy II. Due to the constant flow of ammonia, which is either higher or lower than the flow required for power generation, resulting in a large fluctuation in system efficiency from 23.42% to 99.32% (Fig. 14c).

(4) Strategy IV: Stepped AD-PEMFC-ES

Strategies I-III regulate front-end ammonia flow, while power generation matching is achieved by adjusting the hydrogen valve linked to the PEMFC. Despite stepwise and constant flow rate strategies aiming to minimize ammonia decomposer operation variation, the fuel cell stack's state still fluctuates frequently. Therefore, the strategy utilizing a lithium battery as an energy storage device is proposed to stabilize the

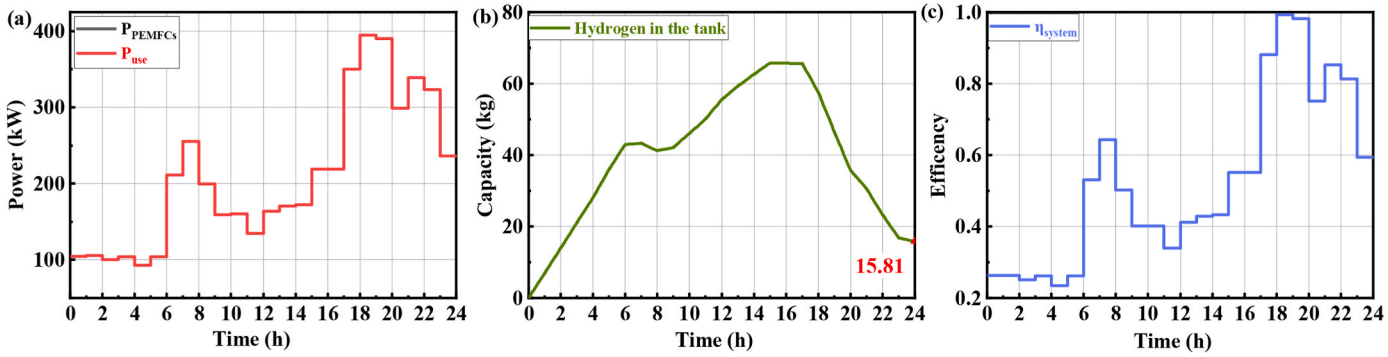


**Fig. 14.** Power of PEMFC Stacks and user, (b) Mass of hydrogen in tank, (c) Efficiency of system.

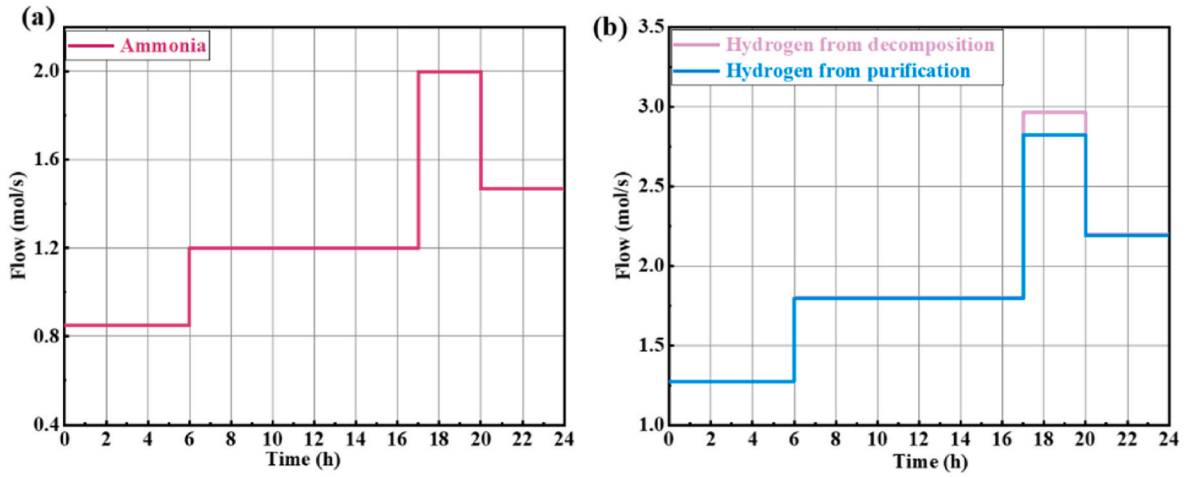


**Fig. 15.** Molar flow (a) Ammonia for AD, (b) Hydrogen production from decomposition and purification.

fuel cell state, completing power generation matching with the assistance of the battery. Firstly, the Strategy IV under the step flow rate is investigated. (Fig. 15).

The power output of the PEMFC stacks varies stepwise with the ammonia feed, because all the hydrogen produced is allocated to the fuel cell stacks. Fig. 16a shows that fuel cell stack I operates at full power, stack II operates in the high-power range, stack III and IV operate almost exclusively at night, and stack IV has a maximum power of only 28 kW, resulting in a low utilization rate. Fuel cell stacks have the same stepped change in efficiency as power (Fig. 16b). Fig. 16c shows that the average power output of stack I, II and III is 44.25%, 46.46% and 41.90% respectively. The electrical efficiency of the three stacks fluctuates between 45% and 60%, which is relatively stable. Stack IV has a low utilization ratio resulting in an average efficiency of 7.03%. The switching times of hydrogen valve is significantly reduced compared to Strategy I, II and III, favoring the lifetime of the fuel cell stacks (Fig. 16d).

Fig. 17a shows the four stages of change in the total power generated by the fuel cell pack: 154 kW, 205 kW, 358 kW and 259 kW. When the power generated by the PEMFC stacks exceeds the power demand, it first meets the user's demand and the remaining power is used to recharge the lithium-ion batteries. Conversely, when the power generated is lower than the power demand, the lithium batteries supplies the user in conjunction with the fuel cell pack. During the all-day operation, 192.75 kWh power is stored (Fig. 17b). The system efficiency remains identical to Strategy II, as the ammonia feed and end-user demand are the same (Fig. 17c).

(5) Strategy V: Constant AD-PEMFC-ES

Strategy IV notably decreases the frequency of condition changes in both the ammonia decomposer and the fuel cell stack. However, maintaining a constant condition is generally preferred, so Strategy V proposes a strategy to keep the main equipment in a constant state relying on lithium battery regulation. The ammonia decomposer and palladium membrane separator in Strategy V are consistent with those in Strategy III (Fig. 18).

Fuel cell stack I, II, and III operated at constant power, while stack IV remained inactive in Fig. 19a. As shown in Fig. 19b, the efficiency of each fuel cell stack is in the high efficiency zone, and the average electrical efficiencies of the three fuel cell stacks were 44.25%, 44.25%, and 57.62% (Fig. 19c). The state of the fuel cell is constant and does not need to be changed (Fig. 19d). Fuel cell stack IV can be removed to reduce investment as it is not switched on. The fuel cell stacks' total generating power remains constant at 218 kW, generation requirement is met mainly by regulating battery (Fig. 20a). Strategy V has a lithium battery storage power of 211.60 kWh, which is 18.85 kWh greater than Strategy IV (Fig. 20b). The system efficiency remains identical to Strategy V, as the ammonia feed and end-user demand are the same (Fig. 20c).

### 4.3. Economic evaluation

The economics of the five strategies in terms of equipment investment costs, fuel costs, power supply revenues, and additional profitable revenues using daily cost as the evaluation metric are provided in Tables 4 and 5.

The average daily costs for Strategy I, II, III, IV and V are 1551.20$, 1481.39$, 1440.78$, 1554.24 $and 1535.50$, respectively. Economic

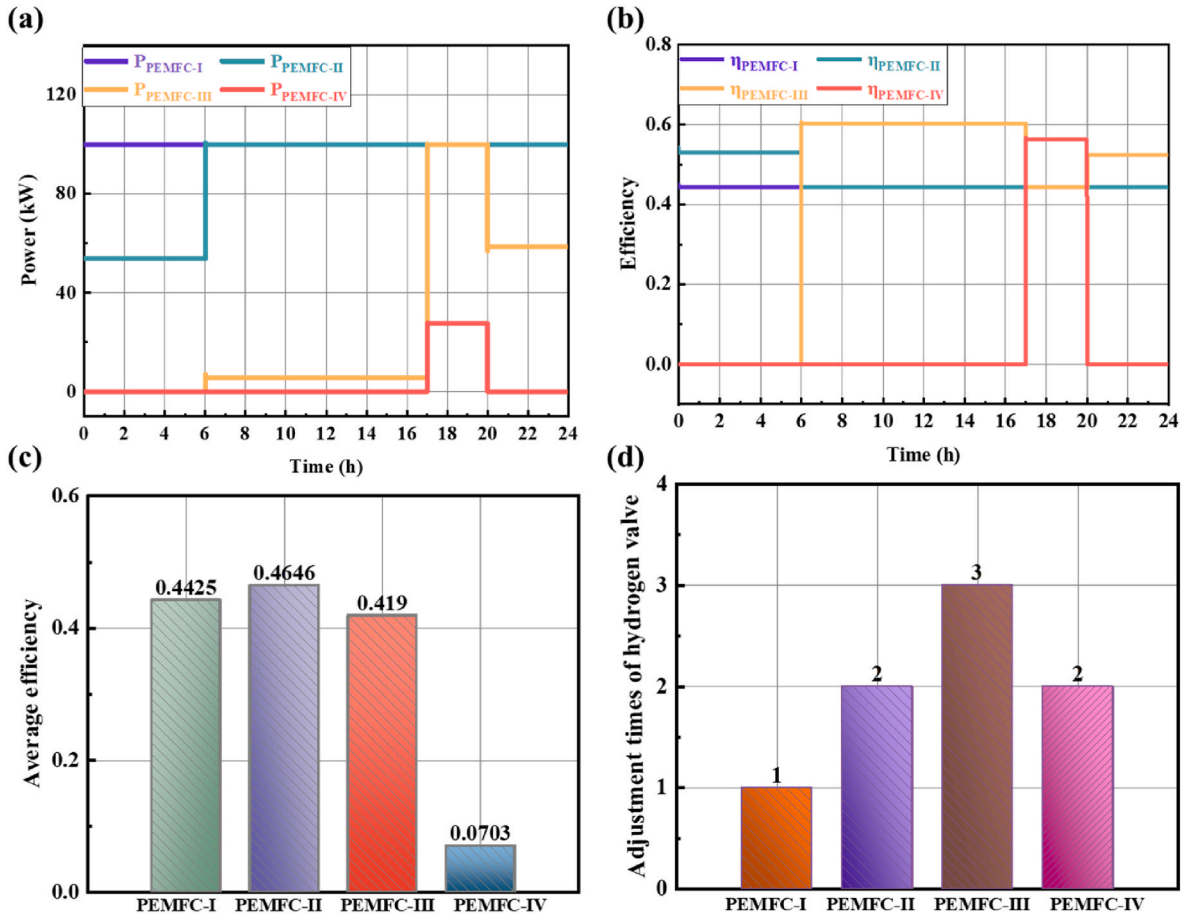


**Fig. 16.** Operating characteristics of the each PEMFC stack (a) Power, (b) Electrical efficiency, (c) Average efficiency, (d) Adjustment times of hydrogen valve.

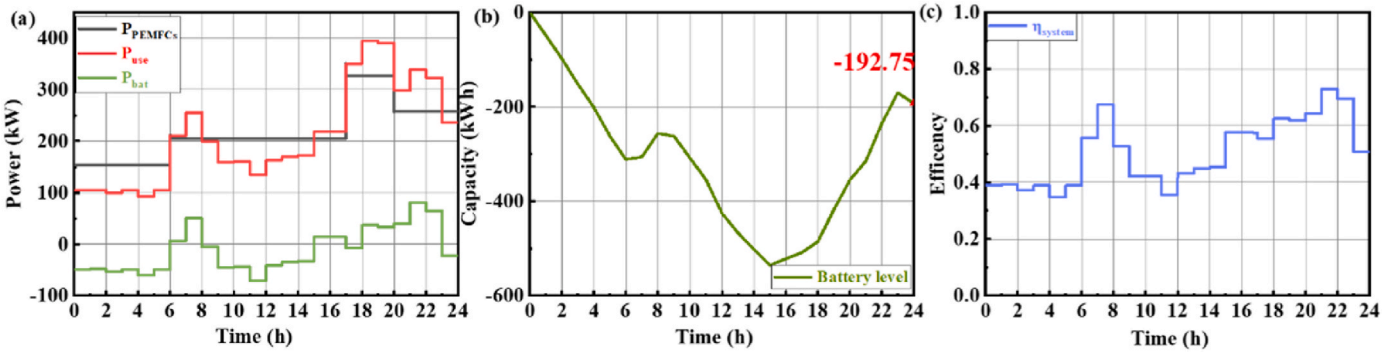


**Fig. 17.** (a) Power of PEMFC Stacks, user and battery, (b) Capacity of battery, (c) Efficiency of system.

analysis of equipment investment, ammonia, power supply, and profitable revenues in Fig. 21 demonstrated that ammonia contributes most to the daily cost, electricity contributes most to the daily revenue regardless of specific strategies. When the constant flow strategy is used, the equipment and maintenance costs are minimized due to the small size of the equipment. By comparing the strategies of the AD-PEMFC-HS and AD-PEMFC-ES, it can be seen that the hydrogen tanks for energy storage reduces the equipment costs by about 7% and increases the profitability since the price of hydrogen is higher than the price of electricity.

### 4.4. Comprehensive evaluation

Considering the fluctuation frequency of ammonia decomposer and fuel cell stacks state, the average system efficiency and the average daily cost (Table 6), the five control strategies were comprehensively assessed. The evaluation indicators included adjustment times, average efficiency of the system, and daily cost. Based on these indicators, Strategy V (Constant AD-PEMFC-ES) was deemed optimal for system control. It was observed that the adjustment times of the ammonia decomposer in Strategy I (Hourly AD-PEMFC) were the highest, being 5 and 20 times higher than those of the stepped and constant flow strategies, respectively. For the four PEMFCs, the highest adjustment times were recorded under Strategy II (Stepped AD-PEMFC-HS) and Strategy III (Constant AD-PEMFC-HS), while they reached a minimum under Strategy IV (Stepped AD-PEMFC-ES) and Strategy V (Constant AD-PEMFC-ES). This reduction was attributed to the configuration of the battery, which decreased the adjustment times of the PEMFCs.

Strategy I demonstrated the highest average system efficiency at

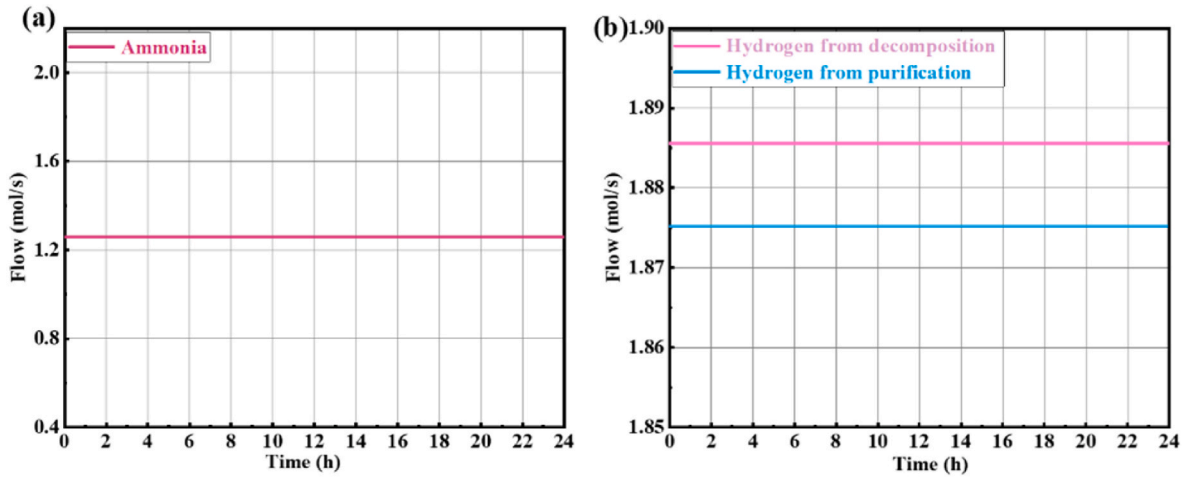


**Fig. 18.** Molar flow (a) Ammonia for AD, (b) Hydrogen production from decomposition and purification.

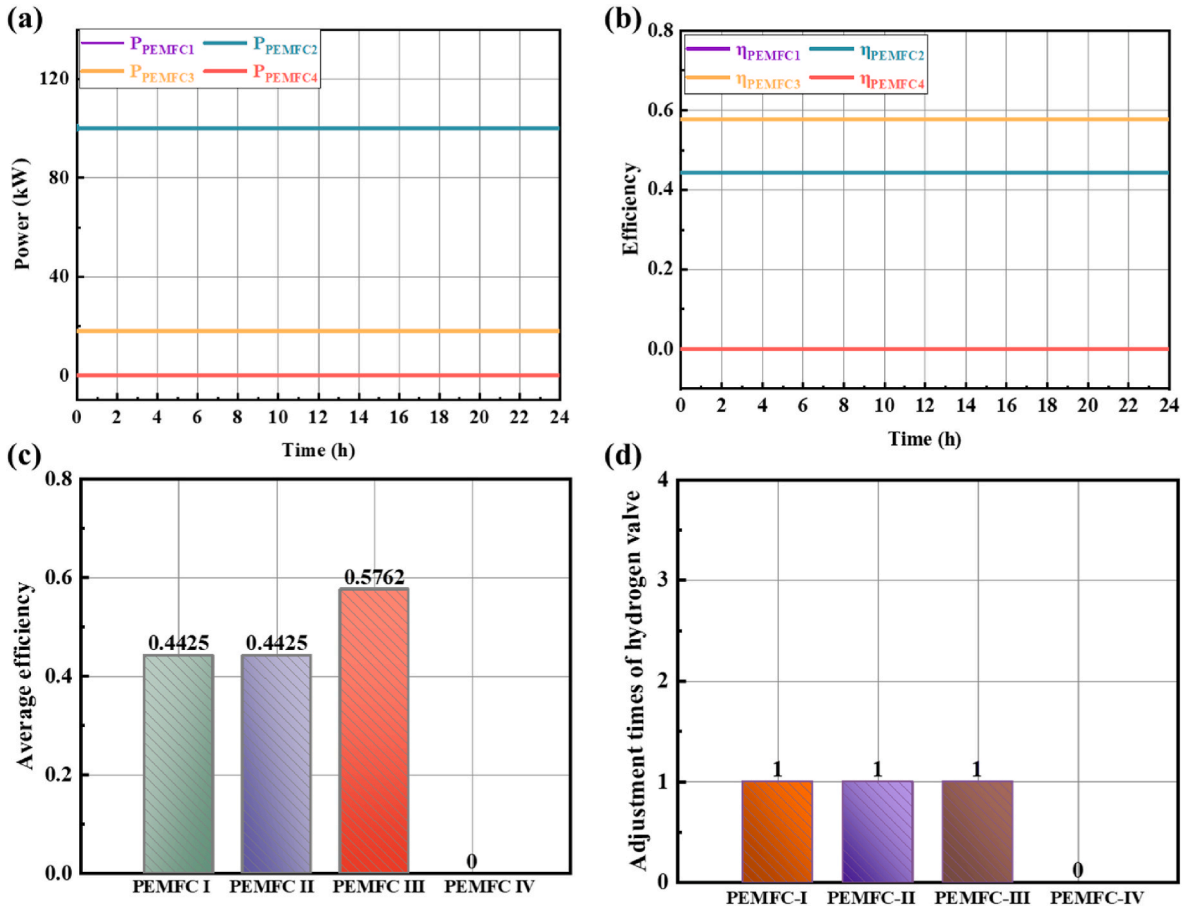


**Fig. 19.** Operating characteristics of the each PEMFC stack (a) Power, (b) Electrical efficiency, (c) Average efficiency, (d) Adjustment times of hydrogen valve.

54.79%, which was 8.75% and 4.38% higher than those of the stepped and constant flow strategies, respectively. This superiority was attributed to the exclusive utilization of hydrogen derived from the regulation of ammonia for power generation, without incorporation of storage or other applications. However, Strategy I comes at the expense of equipment lifespan and overall system stability. This approach may not be conducive to the long-term operation of the power system, as frequent adjustments and high operational demands can accelerate equipment degradation and increase maintenance requirements.

In summary, maintaining constant operating conditions at a constant flow rate is beneficial for equipment lifespan and overall system efficiency. Combining the average daily cost, Strategy V (Constant AD-PEMFC-ES) is deemed optimal, as it balances efficiency and cost-effectiveness, making it the best choice for system control.

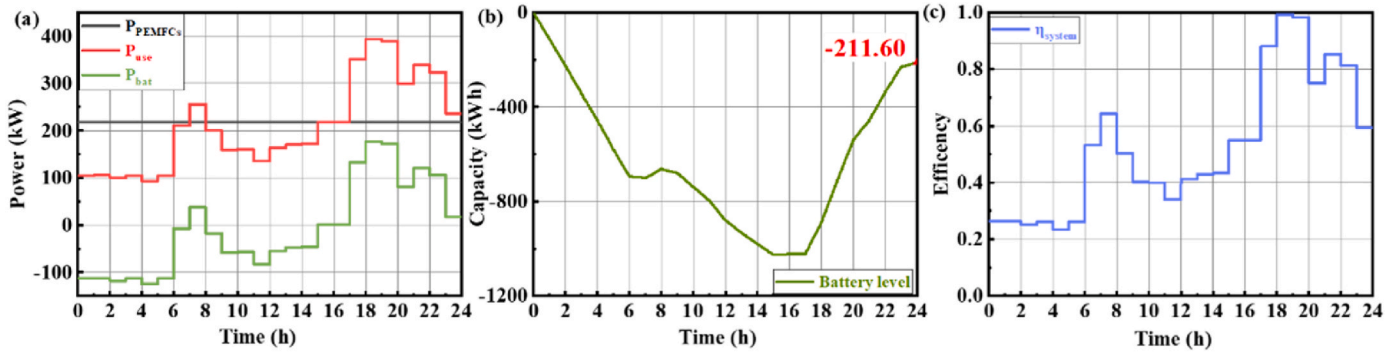


**Fig. 20.** (a) Power of PEMFC Stacks, user and battery, (b) Capacity of battery, (c) Efficiency of system.

**Table 4**
Capacity of the main components in the five strategies.

| Cost Source | Hourly AD-PEMFC | Stepped AD-PEMFC-HS | Constant AD-PEMFC-HS | Stepped AD-PEMFC-ES | Constant AD-PEMFC-ES |
|---|---|---|---|---|---|
| | Capacity | Capacity | Capacity | Capacity | Capacity |
| AD | 250Nm$^3$/h | 250Nm$^3$/h | 180Nm$^3$/h | 250Nm$^3$/h | 180Nm$^3$/h |
| MS | 12.75m$^2$ | 12.75m$^2$ | 9.18m$^2$ | 12.75m$^2$ | 9.18m$^2$ |
| PEMFC | 4 stacks | 4 stacks | 4 stacks | 4 stacks | 3 stacks |
| Storage tank | 15 kg | 11 kg | 16 kg | / | / |
| Battery | / | / | / | 760 kWh | 1390 kWh |
| Ammonia | 1722 kg | 1847 kg | 1847 kg | 1847 kg | 1847 kg |
| Hydrogen | 15 kg | 10.49 kg | 15.81 kg | / | / |
| Electricity | / | / | / | 192.75 kWh | 211.60 kWh |

**Table 5**
Cost of the main components in the five strategies.

| Cost Source | Hourly AD-PEMFC | Stepped AD-PEMFC-HS | Constant AD-PEMFC-HS | Stepped AD-PEMFC-ES | Constant AD-PEMFC-ES |
|---|---|---|---|---|---|
| | Cost ($) | Cost ($) | Cost ($) | Cost ($) | Cost ($) |
| AD | 490 | 490 | 352.80 | 490 | 352.80 |
| MS | 9511.5 | 9511.5 | 6848.28 | 9511.5 | 6848.28 |
| PEMFC | 240000 | 240000 | 240000 | 240000 | 180000 |
| Storage tank | 7500 | 5500 | 8000 | / | / |
| Battery | / | / | / | 25080 | 45870 |
| Ammonia | 1722 | 1847 | 1847 | 1847 | 1847 |
| Hydrogen | 114.15 | 79.83 | 120.31 | / | / |
| Electricity | / | / | / | 15.03 | 16.50 |
| Annual maintenance | 12875.08 | 12775.08 | 12760.05 | 13754.08 | 11653.55 |
| Average daily cost | 1551.20 | 1481.39 | 1440.78 | 1554.24 | 1535.50 |

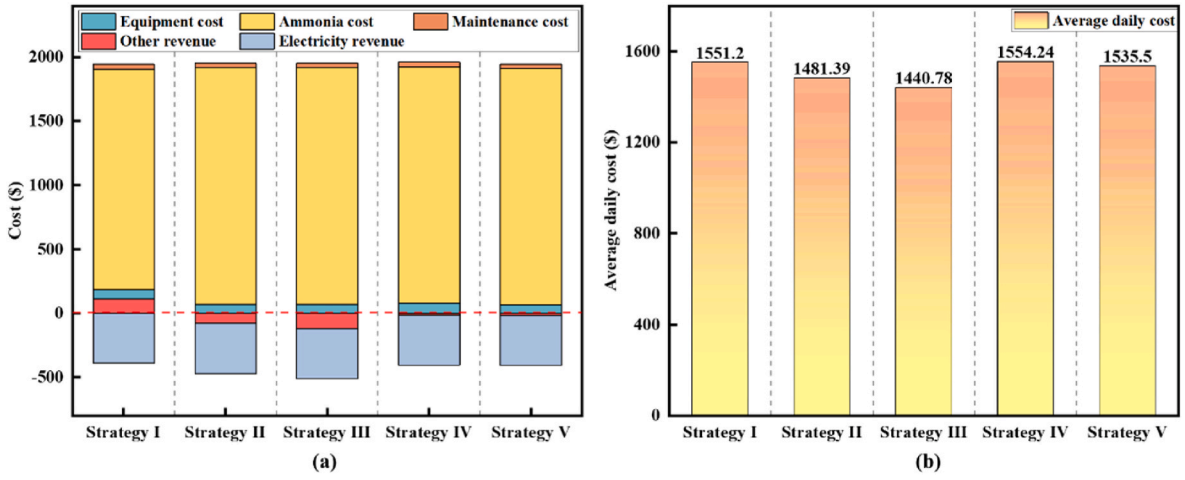


**Fig. 21.** Economic evaluation of the system (a) Cost of the main components under five strategies, (b) The average daily cost of the five strategies.

**Table 6**
Comparison of control strategies across various evaluation indicators.

| Strategy | Adjustment times of ammonia decomposer | Adjustment times of PEMFCs | Average efficiency of system | Average daily cost |
|---|---|---|---|---|
| Hourly AD-PEMFC | 21 | 30 | 54.79% | 1551.20$ |
| Stepped AD-PEMFC-HS | 4 | 32 | 50.38% | 1481.39$ |
| Constant AD-PEMFC-HS | 1 | 32 | 52.49% | 1440.78$ |
| Stepped AD-PEMFC-ES | 4 | 8 | 50.38% | 1554.24$ |
| Constant AD-PEMFC-ES | 1 | 3 | 52.49% | 1535.50$ |

## 5. Conclusions and future work

In this study, a PEMFC power generation system based on ammonia catalytic decomposition is proposed, which considers the main working components such as ammonia decomposer, membrane separator and PEMFC. With the 24 hours electricity demand of 285 households as the control target, five control strategies are proposed, considering different operation modes of hourly, stepped and constant hydrogen flow. Different energy storage devices including hydrogen storage tanks and lithium battery are used for peak power generation in support of PEMFC power generation. This system not only meets user demands but also ensures stable hydrogen production and power generation, achieving high electrical efficiency and zero greenhouse gas emissions. The evaluation of five control strategies reveals that the hourly AD-PEMFC control strategy can achieve an electrical efficiency of up to 54.79% through controlled hydrogen production and coordinated regulation of the fuel cell and energy storage devices. However, frequent fluctuations in the ammonia decomposer can hinder system smoothness. The constant AD-PEMFC-HS strategy achieves the lowest daily average cost of $1440.78 but involves the highest number of fuel cell hydrogen valve adjustments, which is detrimental to the stable operation of the PEMFCs. Meanwhile, the constant AD-PEMFC-ES strategy, which requires one adjustment for the ammonia valve and three adjustments for the hydrogen valve, exhibits an efficiency of 52.49% and is deemed the optimal strategy for extending equipment lifetime and enhancing overall system efficiency.

It is important to acknowledge that the results of this study may require further validation in practical settings, beyond the limitations and assumptions of the simulation models. The performance and computational results of different strategies may vary significantly depending on the electricity load curves of different seasons or user groups. The fuel cell power generation system based on ammonia decomposition is influenced by many critical factors. The daily average cost is composed of multiple factors, such as hydrogen price, hydrogen storage tank price, and operation and maintenance costs. These factors are subject to annual variations, which may lead to different economic evaluation results. Future research will fully consider the aforementioned factors to provide a more comprehensive and accurate assessment.

## CRediT authorship contribution statement

**Jiale Yan:** Writing – original draft, Visualization, Validation, Investigation, Formal analysis, Data curation. **Jiong Wang:** Visualization, Validation, Formal analysis, Data curation. **Shanshan Cai:** Writing – review & editing, Project administration, Methodology, Conceptualization. **Chunyan Zang:** Writing – review & editing, Validation, Supervision, Resources, Project administration, Methodology, Conceptualization. **Song Li:** Writing – review & editing, Supervision, Resources, Project administration, Methodology, Funding acquisition, Formal analysis, Conceptualization. **Zhengkai Tu:** Supervision, Project administration, Methodology.

## Declaration of competing interest

The authors declare that they have no known competing financial interests or personal relationships that could have appeared to influence the work reported in this paper.

## Acknowledgments

This work was supported by National Key Research and Development Program (No. 2022YFB4003704).

## References

[1] Khan I, Zakari A, Zhang J, Dagar V, Singh S. A study of trilemma energy balance, clean energy transitions, and economic expansion in the midst of environmental sustainability: new insights from three trilemma leadership. Energy 2022;248:123619. https://doi.org/10.1016/j.energy.2022.123619.
[2] Jeje SO, Marazani T, Obiko JO, Shongwe MB. Advancing the hydrogen production economy: a comprehensive review of technologies, sustainability, and future prospects. Int J Hydrogen Energy 2024;78:642–61. https://doi.org/10.1016/j.ijhydene.2024.06.344.
[3] Trattner A, Klell M, Radner F. Sustainable hydrogen society-Vision, findings and development of a hydrogen economy using the example of Austria. Int J Hydrogen Energy 2022;47:2059–79. https://doi.org/10.1016/j.ijhydene.2021.10.166.
[4] Yazdi M, Zarei E, Pirbalouti RG, Li H. A comprehensive resilience assessment framework for hydrogen energy infrastructure development. Int J Hydrogen Energy 2024;51:928–47. https://doi.org/10.1016/j.ijhydene.2023.06.271.
[5] Ahmad S, Ullah A, Samreen A, Qasim M, Nawaz K, Ahmad W, et al. Hydrogen production, storage, transportation and utilization for energy sector: a current status review. J Energy Storage 2024;101:113733. https://doi.org/10.1016/j.est.2024.113733.
[6] Devkota S, Cha J-Y, Shin B-J, Mun J-H, Yoon HC, Mazari SA, et al. Techno-economic and environmental assessment of hydrogen production through ammonia decomposition. Appl Energy 2024;358:122605. https://doi.org/10.1016/j.apenergy.2023.122605.
[7] Tawalbeh M, Murtaza SZM, Al-Othman A, Alami AH, Singh K, Olabi AG. Ammonia: a versatile candidate for the use in energy storage systems. Renew Energy 2022;194:955–77. https://doi.org/10.1016/j.renene.2022.06.015.
[8] Zhu G, Tian Y, Liu M, Zhao Y, Wang W, Wang M, et al. Comprehensive competitiveness assessment of ammonia-hydrogen fuel cell electric vehicles and their competitive routes. Energy 2023;285:129471. https://doi.org/10.1016/j.energy.2023.129471.
[9] Geraldo de Melo Furtado J, Gatti GC, Serra ET, Anibal de Almeida SC. Performance analysis of a 5 kW PEMFC with a natural gas reformer. Int J Hydrogen Energy 2010;35:9990–5. https://doi.org/10.1016/j.ijhydene.2010.02.042.
[10] Novoa L, Neal R, Samuelsen S, Brouwer J. Fuel cell transmission integrated grid energy resources to support generation-constrained power systems. Appl Energy 2020;276:115485. https://doi.org/10.1016/j.apenergy.2020.115485.
[11] Xu D, Liu Q, Lei J, Jin H. Performance of a combined cooling heating and power system with mid-and-low temperature solar thermal energy and methanol decomposition integration. Energy Convers Manag 2015;102:17–25. https://doi.org/10.1016/j.enconman.2015.04.014s.
[12] Afif A, Radenahmad N, Cheok Q, Shams S, Kim JH, Azad AK. Ammonia-fed fuel cells: a comprehensive review. Renew Sustain Energy Rev 2016;60:822–35. https://doi.org/10.1016/j.rser.2016.01.120.
[13] Miyaoka H, Miyaoka H, Ichikawa T, Ichikawa T, Kojima Y. Highly purified hydrogen production from ammonia for PEM fuel cell. Int J Hydrogen Energy 2018;43:14486–92. https://doi.org/10.1016/j.ijhydene.2018.06.065.
[14] Cinti G, Liso V, Sahlin SL, Araya SS. System design and modeling of a high temperature PEM fuel cell operated with ammonia as a fuel. Energies 2020;13. https://doi.org/10.3390/en13184689.
[15] Meng T, Cui D, Shi Y, Ji Y, Cheng M, Tu B, et al. Performance evaluation of high-efficiency SOFC-PEMFC hybrid system fueled by liquid ammonia. Int J Hydrogen Energy 2023;48:30887–98. https://doi.org/10.1016/j.ijhydene.2023.04.222.
[16] Duong PA, Ryu BR, Lee H, Kang H. Thermodynamic analysis of integrated ammonia fuel cells system for maritime application. Energy Rep 2023;10:1521–37. https://doi.org/10.1016/j.egyr.2023.08.028.
[17] Xu J-H, Zhang B-X, Yan H-Z, Ding Q, Zhu K-Q, Yang Y-R, et al. A comprehensive assessment of the hybrid power generation system of PEMFC and internal

combustion engine based on ammonia decomposition. Energy 2023;285:129559. https://doi.org/10.1016/j.energy.2023.129559.
[18] Gong C, Xu Y, Cai S, Chi B, Tu Z. Comparative study on thermodynamic analysis of solid oxide fuel cells supplied with methanol or ammonia. Int J Hydrogen Energy 2024;50:1293–301. https://doi.org/10.1016/j.ijhydene.2023.10.266.
[19] Nie Z, Huang Y, Lu Z, Tian G, Liu X. Energy efficiency analysis of ammonia-fueled power systems for vehicles considering residual heat recovery. Energy 2024;312:133338. https://doi.org/10.1016/j.energy.2024.133338.
[20] Wang Z, Dong B, Yin J, Li M, Ji Y, Han F. Towards a marine green power system architecture: integrating hydrogen and ammonia as zero-carbon fuels for sustainable shipping. Int J Hydrogen Energy 2024;50:1069–87. https://doi.org/10.1016/j.ijhydene.2023.10.207.
[21] Ezzat M, Dincer I. Exergoeconomic analysis and optimization of a new hybrid fuel cell vehicle. Int J Hydrogen Energy 2020;45:5734–44. https://doi.org/10.1016/j.ijhydene.2019.07.104.
[22] Yu Y, Luo C, Min H, Cao Q, Jiang J, Wu H. Role of proton exchange membrane fuel cell in efficiency improvement of ammonia-hydrogen fusion zero-carbon powertrains for long-haul, heavy-duty transportation. Energy Convers Manag 2024;309. https://doi.org/10.1016/j.enconman.2024.118425.
[23] Peng F, Zhao Y, Li X, Liu Z, Chen W, Liu Y, et al. Development of master-slave energy management strategy based on fuzzy logic hysteresis state machine and differential power processing compensation for a PEMFC-LIB-SC hybrid tramway. Appl Energy 2017;206:346–63. https://doi.org/10.1016/j.apenergy.2017.08.128.
[24] Wang T, Li Q, Yin L, Chen W. Hydrogen consumption minimization method based on the online identification for multi-stack PEMFCs system. Int J Hydrogen Energy 2019;44:5074–81. https://doi.org/10.1016/j.ijhydene.2018.09.181.
[25] Fathy A, Abdelkareem MA, Olabi AG, Rezk H. A novel strategy based on salp swarm algorithm for extracting the maximum power of proton exchange membrane fuel cell. Int J Hydrogen Energy 2021;46:6087–99. https://doi.org/10.1016/j.ijhydene.2020.02.165.
[26] Yuan Y, Chen L, Lyu X, Ning W, Liu W, Tao W-Q. Modeling and optimization of a residential PEMFC-based CHP system under different operating modes. Appl Energy 2024;353:122066. https://doi.org/10.1016/j.apenergy.2023.122066.
[27] Cai S, Wang W, Zou Y, Li S, Tu Z. Performance and sustainability assessment of PEMFC/solar-driven CCP systems with different energy storage devices. Energy 2023;278:127863. https://doi.org/10.1016/j.energy.2023.127863.
[28] Cesaro Z, Ives M, Nayak-Luke R, Mason M, Banares-Alcantara R. Ammonia to power: forecasting the levelized cost of electricity from green ammonia in large-scale power plants. Appl Energy 2021;282:116009. https://doi.org/10.1016/j.apenergy.2020.116009.
[29] Shahverdian MH, Sohani A, Pedram MZ, Sayyaadi H. An optimal strategy for application of photovoltaic-wind turbine with PEMEC-PEMFC hydrogen storage system based on techno-economic, environmental, and availability indicators. J Clean Prod 2023;384:135499. https://doi.org/10.1016/j.jclepro.2022.135499.
[30] Chen Y, Lu J, Liu Z, Liu Y, Huang T, Ren X, et al. Comprehensive evaluation on a heat self-balanced low-temperature ammonia reforming-based high-power hybrid power generation system combined with proton exchange membrane fuel cell and internal combustion engine. J Clean Prod 2025:144755. https://doi.org/10.1016/j.jclepro.2025.144755.
[31] Lin L, Sun M, Wu Y, Huang W, Wu Z, Wang D, et al. High-efficiency ammonia-fueled hybrid power generation system combining ammonia decomposition, proton exchange membrane fuel cell and micro gas turbine: a thermodynamic model and performance optimization. Energy Convers Manag 2025;325:119358. https://doi.org/10.1016/j.enconman.2024.119358.
[32] Zhang Y, Zhao N, Li M, Xu Z, Wu D, Hillmansen S, et al. A techno-economic analysis of ammonia-fuelled powertrain systems for rail freight. Transport Res Transport Environ 2023;119:103739. https://doi.org/10.1016/j.trd.2023.103739.
[33] Di Micco S, Cigolotti V, Mastropasqua L, Brouwer J, Minutillo M. Ammonia-powered ships: concept design and feasibility assessment of powertrain systems for a sustainable approach in maritime industry. Energy Convers Manag X 2024;22:100539. https://doi.org/10.1016/j.ecmx.2024.100539.
[34] Chang H, Xu X, Shen J, Shu S, Tu Z. Performance analysis of a micro-combined heating and power system with PEM fuel cell as a prime mover for a typical household in North China. Int J Hydrogen Energy 2019;44:24965–76. https://doi.org/10.1016/j.ijhydene.2019.07.183.
[35] Nasharuddin R, Zhu M, Zhang Z, Zhang D. A technoeconomic analysis of centralised and distributed processes of ammonia dissociation to hydrogen for fuel cell vehicle applications. Int J Hydrogen Energy 2019;44:14445–55. https://doi.org/10.1016/j.ijhydene.2019.03.274.
[36] Andriani D, Bicer Y. A review of hydrogen production from onboard ammonia decomposition: maritime applications of concentrated solar energy and boil-off gas recovery. Fuel 2023;352. https://doi.org/10.1016/j.fuel.2023.128900.
[37] Hua TQ, Ahluwalia RK, Peng JK, Kromer M, Lasher S, McKenney K, et al. Technical assessment of compressed hydrogen storage tank systems for automotive applications. Int J Hydrogen Energy 2011;36:3037–49. https://doi.org/10.1016/j.ijhydene.2010.11.090.
[38] Al-Hamed KHM, Dincer I. A novel ammonia solid oxide fuel cell-based powering system with on-board hydrogen production for clean locomotives. Energy 2021;220:119771. https://doi.org/10.1016/j.energy.2021.119771.
[39] Um DH, Kim TY, Kwon OC. Power and hydrogen production from ammonia in a micro-thermophotovoltaic device integrated with a micro-reformer. Energy 2014;73:531–42. https://doi.org/10.1016/j.energy.2014.06.053.
[40] Djéga-Mariadassou G, Shin CH, Bugli G. Tamaru's model for ammonia decomposition over titanium oxynitride. J Mol Catal Chem 1999;141:263–7. https://doi.org/10.1016/s1381-1169(98)00270-2.
[41] Wang W, Herreros JM, Tsolakis A, York APE. Ammonia as hydrogen carrier for transportation; investigation of the ammonia exhaust gas fuel reforming. Int J Hydrogen Energy 2013;38:9907–17. https://doi.org/10.1016/j.ijhydene.2013.05.144.
[42] Di Marcoberardino G, Binotti M, Manzolini G, Viviente JL, Arratibel A, Roses L, et al. Achievements of European projects on membrane reactor for hydrogen production. J Clean Prod 2017;161:1442–50. https://doi.org/10.1016/j.jclepro.2017.05.122.
[43] Tang X-Y, Yang W-W, Ma X, Cao XE. An integrated modeling method for membrane reactors and optimization study of operating conditions. Energy 2023;268:126730. https://doi.org/10.1016/j.energy.2023.126730.
[44] Xie D, Lu N, Wang F, Fan S. Calculation of the hydrogen production rate by a palladium membrane separator: theoretical approaches. Int J Hydrogen Energy 2013;38:10802–12. https://doi.org/10.1016/j.ijhydene.2013.01.018.
[45] Zhao J, Chang H, Luo X, Tu Z, Chan SH. Dynamic analysis of a CCHP system based on fuel cells integrated with methanol-reforming and dehumidification for data centers. Appl Energy 2022;309:118496. https://doi.org/10.1016/j.apenergy.2021.118496.
[46] Sandoval C, Alvarado VM, Carmona J-C, Lopez Lopez G, Gomez-Aguilar JF. Energy management control strategy to improve the FC/SC dynamic behavior on hybrid electric vehicles: a frequency based distribution. Renew Energy 2017;105:407–18. https://doi.org/10.1016/j.renene.2016.12.029.
[47] He L, Hu X, Yin G, Shao X, Liu J, Shi Q. A voltage dynamics model of lithium-ion battery for state-of-charge estimation by proportional-integral observer. Appl Energy 2023;351:121793. https://doi.org/10.1016/j.apenergy.2023.121793.
[48] Chen M, Rincon-Mora GA. Accurate electrical battery model capable of predicting, runtime and I-V performance. IEEE Trans Energy Convers 2006;21:504–11. https://doi.org/10.1109/tec.2006.874229.
[49] Wang Y, Zhang H, He S, Wang W, Gao M, Moiseevna KE, et al. Dynamic analysis and control optimization of hydrogen supply for the proton exchange membrane fuel cell and metal hydride coupling system with a hydrogen buffer tank. Energy Convers Manag 2023;291:117339. https://doi.org/10.1016/j.enconman.2023.117339.
[50] Chen L, Xu K, Yang Z, Yan Z, Dong Z. Optimal design and operation of dual-ejector PEMFC hydrogen supply and circulation system. Energies 2022;15:155427. https://doi.org/10.3390/en15155427.
[51] An E, Zhang W. Tech-economic analysis of ammonia as hydrogen carrier for transportation and production. J Tongji Univ Nat Sci 2010;38:1371–4. https://doi.org/10.3969/j.issn.0253-374x.2010.09.023.
[52] Sangtongkitcharoen W, Vivanpatarakij S, Laosiripojana N, Arpornwichanop A, Assabumrungrat S. Performance analysis of methanol-fueled solid oxide fuel cell system incorporated with palladium membrane reactor. Chem Eng J 2008;138:436–41. https://doi.org/10.1016/j.cej.2007.06.021.
[53] Perčić M, Vladimir N, Jovanović I, Koričan M. Application of fuel cells with zero-carbon fuels in short-sea shipping. Appl Energy 2022;309:118463. https://doi.org/10.1016/j.apenergy.2021.118463.
[54] Shin HK, Ha SK. A review on the cost analysis of hydrogen gas storage tanks for fuel cell vehicles. Energies 2023;16:135223. https://doi.org/10.3390/en16135233.
[55] Martins AH, Rouboa A, Monteiro E. On the green hydrogen production through gasification processes: a techno-economic approach. J Clean Prod 2023;383:135476. https://doi.org/10.1016/j.jclepro.2022.135476.
[56] Chen X, Zhou H, Li W, Yu Z, Gong G, Yan Y, et al. Multi-criteria assessment and optimization study on 5 kW PEMFC based residential CCHP system. Energy Convers Manag 2018;160:384–95. https://doi.org/10.1016/j.enconman.2018.01.050.
[57] Chellappa AS, Fischer CM, Thomson WJ. Ammonia decomposition kinetics over Ni-Pt/$Al_2O_3$ for PEM fuel cell applications. Appl Catal, A 2002;227:231–40. https://doi.org/10.1016/s0926-860x(01)00941-3.
[58] Xie D, Wang F, Wu K, Zhang E, Zhang Y. Permeation efficiency of Pd-Ag membrane modules with porous stainless steel substrates. Sep Purif Technol 2012;89:189–92. https://doi.org/10.1016/j.seppur.2012.01.030.
[59] Wan Z, Shen J, Zhang H, Tu Z, Liu W. In situ temperature measurement in a 5 kW-class Proton Exchange Membrane Fuel Cell stack with pure oxygen as the oxidant. Int J Heat Mass Tran 2014;75:231–4. https://doi.org/10.1016/j.ijheatmasstransfer.2014.03.075.